

Biophysical and biochemical characterization of yeast tRNA nucleotidyltransferase variants

Mohammed Samiur Rahman

A Thesis in
The Department of
Chemistry and Biochemistry

Presented in Partial Fulfillment of the Requirements for
The Degree of Master of Science (Biochemistry)
At Concordia University
Montreal, Quebec, Canada

December 2017

©Mohammed Samiur Rahman

By: **Mohammed Samiur Rahman**

Entitled: **Biophysical and biochemical characterization of yeast tRNA
nucleotidyltransferase variants**

Submitted in partial fulfillment of the requirements for the degree of
Master of Science (Biochemistry)

Complies with the regulations of the University and meets the accepted standards
with respect to originality and quality.

Signed by the final Examining Committee:

Dr. Paul Joyce _____ **Thesis Supervisor**

Dr. Justin Powlowski _____ **Examiner**

Dr. Peter Pawelek _____ **Examiner**

Dr. Gilles Peslherbe _____ **Chair**

Approved by: Dr. Peter Pawelek _____ **Graduate Program Director**

Dr. André Roy _____ **Dean of Faculty**

Date: December 2017

ABSTRACT

Biophysical and biochemical characterization of yeast tRNA nucleotidyltransferase variants

Mohammed Samiur Rahman, MSc

Concordia University, 2017

The enzyme ATP(CTP):tRNA-specific tRNA nucleotidyltransferase adds cytidine-cytidine-adenosine (CCA) to the 3' end of eukaryotic tRNAs during their maturation. This CCA sequence plays a vital role in aminoacylation and hence in protein synthesis. In yeast, this enzyme is defined as a Class II tRNA nucleotidyltransferase due to the presence of five conserved N-terminal motifs (A to E). Based on the available crystal structures of related tRNA nucleotidyltransferases, specific functions have been assigned to each of these motifs. We previously have shown that mutations in motif C that reduce enzyme activity can be overcome by a mutation in motif A that restores this activity. Here we explore the roles of two acidic residues (glutamate 189 and aspartate 190) found within motif C and one residue (arginine 64) found in motif A to understand better the role of motif C and the potential interactions between motifs A and C.

Site-directed mutagenesis was used to change arginine 64 (to tryptophan), or glutamate 189 (to glutamine, lysine, alanine or phenylalanine) or aspartate 190 (to alanine or phenylalanine) alone, or in combination with the arginine 64 tryptophan substitution and the effects of these amino acid alterations on enzyme structure and function were studied. Biophysical analyses (circular dichroism and fluorescence spectroscopy and thermal denaturation experiments) suggest no major changes in structure in almost all of the variants tested. Kinetic analysis revealed no alterations in substrate binding (K_m), but a large drop in turnover number (k_{cat}) for the 189 and 190 variants (but not the arginine 64 variant). The reduced activity in the 189 and 190 variants is alleviated when accompanied by the change of arginine 64 to tryptophan, which also suppresses the temperature-sensitive phenotype. Taken together these data suggest that arginine 64 is not required for enzyme activity unlike glutamate 189 and aspartate 190. Moreover, they suggest an interaction between motifs A and C, and that motif C plays a role in accommodating and orienting the substrates to promote catalysis involving motif A.

ACKNOWLEDGMENTS

Special thanks to Dr. Paul Joyce for providing me with this wonderful opportunity to work with his research team and in this project. His guidance and patience with me helped in the completion of this project. Pam was very helpful with the obstacles involving molecular biology faced in this project and in her, I found a great teacher. Thanks to Matthew for training me from the beginning of this project. Also, thanks to Tian and Michael for their support.

I convey my appreciation to Dr. Justin Powlowski and Dr. Peter Pawelek for giving me their valuable time being in my committee, hearing out my project ideas and helping towards its completion. Special thanks to Dr. Joanne Turnbull and Dr. Judith Kornblatt for their expertise regarding enzyme kinetics and circular dichroism spectroscopy.

I would also like to thank my wonderful parents Salma and Mahfuz, and beloved younger sister Anika for their support in boosting my spirit to have a proper mindset and motivation in carrying out my Master's studies. Lastly, my dear love Mahtab, whose phenomenal presence brought brightness to my life, illuminating the correct path at every step while activating the best in me.

Mohammed Samiur Rahman

TABLE OF CONTENTS

ABSTRACT.....	iii
ACKNOWLEDGMENTS.....	iv
LIST OF FIGURES.....	vii
LIST OF TABLES	ix
LIST OF ABBREVIATIONS	x
1.0 INTRODUCTION.....	1
1.1 Conserved motifs of Class II tRNA nucleotidyltransferases	1
1.1.1 Motif A	5
1.1.2 Motif B	6
1.1.3 Motif C	6
1.1.4 Motif D	10
1.1.5 Motif E.....	11
1.1.6 The carboxy terminal body and tail domain	12
1.2 Project Objectives.....	13
2.0 MATERIALS AND METHODS.....	14
2.1 Strains, Buffers, Growth Media, and Solutions.....	14
2.2 Construction of Expression System	18
2.3 Expression and purification of yeast tRNA nucleotidyltransferase proteins	19
2.3.1 Protein Expression (modified from Shan <i>et al.</i> , 2008).....	19
2.3.2 Cell Lysis (modified from Shan <i>et al.</i> , 2008).....	19
2.3.3 GST-tagged affinity column (Harper <i>et al.</i> , 2011)	20
2.3.4 Purification, thrombin cleavage and dialysis (modified from Shan <i>et al.</i> , 2008).....	20
2.3.5 Sodium dodecyl sulfate polyacrylamide gel electrophoresis (SDS-PAGE) (modified from Sambrook <i>et al.</i> , 1989)	21
2.3.6 Protein Concentration determination.....	21
2.4 Biophysical Characterization of yeast tRNA nucleotidyltransferase	22
2.4.1 Circular Dichroism Spectroscopy	22
2.4.2 Fluorescence Spectrophotometry	23
2.4.3 Fluorescence Quenching of native and R64W proteins using ATP or CTP (modified from Shan <i>et al.</i> , 2008).....	23
2.5 Enzyme Activity Assays	24
2.5.1 Run-off transcription and purification of transcripts.....	24
2.5.2 Measuring nucleotide addition	25
2.5.3 Standard Activity Assays.....	25
2.5.4 Standard Kinetic Assays	26
2.5.5 Standard Activity Assay with variable metal ions and to investigate NTP misincorporation	26
2.6 Molecular modeling and visualization	27

2.7 Proteolysis Experiments	27
3.0 RESULTS.....	28
3.1 Characterization of growth phenotypes.....	28
3.2 Protein Purification.....	30
3.3 Biophysical Characterization of native and variant tRNA-NT enzymes	33
3.3.1 Effect of amino acid substitutions at positions 64, 189 and 190 on circular dichroism spectra	33
3.3.2 Effect of amino acid substitutions at positions 64, 189 and 190 on thermal stability	35
3.4 Effect of amino acid substitutions at positions 64, 189 and 190 on intrinsic fluorescence	37
3.5 Effect of amino acid substitutions at positions 64, 189 and 190 on enzyme activity	40
3.6 Role of metal ions in defining recognition of ATP or CTP in native and R64W enzymes	49
3.7 Nucleotide triphosphate substrate specificity with Mg ²⁺ or Ca ²⁺ ions in native and R64W enzymes	53
3.8 Fluorescence quenching of tryptophan fluorescence in the native and R64W proteins by ATP or CTP to determine K _d	55
3.9 Proteolysis	57
3.9.1 SDS-PAGE Results of Proteolysis with Chymotrypsin	57
3.9.2 Identifying the new chymotryptic cleavage site	59
4.0 DISCUSSION	60
4.1 The role of motif C.....	60
4.2 The role of R64 in enzyme function	66
5.0 CONCLUSION AND FUTURE WORKS	75
6.0 REFERENCES.....	78
7.0 APPENDIX	81

LIST OF FIGURES

- 1-1:** Crystal structures of class II tRNA nucleotidyltransferases
- 1-2:** Alignment of five class II tRNA nucleotidyltransferase sequences from different organisms
- 1-3:** Model of *Saccharomyces cerevisiae* tRNA nucleotidyltransferase
- 1-4:** Reaction scheme for addition at motif A of a nucleoside triphosphate to a tRNA
- 1-5:** Replica plating results to identify temperature-sensitive mutants of the *CCA1* gene
- 1-6:** Nucleotide addition by tRNA nucleotidyltransferase variants
- 1-7:** Mechanistic model for different motif C states during CCA-addition
- 1-8:** Interactions between the *Bacillus stearothermophilus* CCA-adding enzyme and tRNA
- 3-1:** Growth of yeast expressing native and variant tRNA nucleotidyltransferases
- 3-2:** Purification of native tRNA nucleotidyltransferase
- 3-3:** Level of purity of native and variant tRNA nucleotidyltransferases used in this study
- 3-4:** Overlay of peptide backbone scans of native and variant tRNA nucleotidyltransferases
- 3-5:** Overlay of thermal denaturation profiles of native and variant tRNA nucleotidyltransferases defined using circular dichroism spectroscopy
- 3-6:** Overlay of fluorescence emission spectra for native and variant tRNA nucleotidyltransferases excited at 280 nm and 295 nm
- 3-7:** Qualitative enzyme activity assays on native and variant tRNA nucleotidyltransferases
- 3-8:** Incorporation of AMP and/or CMP in the presence of different divalent cations
- 3-9:** Nucleotide specificity of the native and R64W proteins using either Mg^{2+} or Ca^{2+} as cofactor
- 3-10:** Fluorescence Quenching of native and R64W enzymes with ATP or CTP
- 3-11:** Proteolysis of native and variant tRNA nucleotidyltransferases using α -chymotrypsin
- 4-1:** The region adjacent to the residue corresponding to *S. cerevisiae* Glu189 in the crystal structures of *A. aeolicus*, *B. stearothermophilus* and human tRNA nucleotidyltransferases
- 4-2:** Proposed structural model derived from the comparison of the differences between native and D139A variant human tRNA nucleotidyltransferase as revealed after a 7.5 ns MD simulation (YASARA)
- 4-3:** ClustalW alignment of tRNA nucleotidyltransferase sequences optimized manually

4-4: Conserved motifs of yeast tRNA nucleotidyltransferases showing portions of the head and neck domain

4-5: Alignment of the region around motif A in five class II tRNA nucleotidyltransferase sequences from different organisms

4-6: Hydrogen bond Interactions of Arg31 and Ala52 to form part of the only β -sheet found in the human tRNA nucleotidyltransferase

7-1: BSA standard curve to determine the concentrations of the native and variant tRNA nucleotidyltransferases

7-2: Michaelis-Menten graphs of native enzyme using tRNA, CTP or ATP as variable substrate to determine kinetic parameters

7-3: Determination of dissociation constant of native tRNA nucleotidyltransferase using fluorescence quenching with ATP or CTP

7-4: Gel images showing excision of bands of interest before trypsin digestion and mass spectrometric (Orbitrap) analysis

7-5: Mass spectrometric results generated from SEQUEST search carried out against the *S. cerevisiae* proteome database from UniProt

7-6: Possible cleavage sites of α -chymotrypsin in native tRNA nucleotidyltransferase

7-7: Models of native and R64W tRNA nucleotidyltransferases to investigate the possible chymotryptic cleavage site using PyMOL

LIST OF TABLES

2-1: Components for Buffers, Solutions and Growth Media

2-2: Suppliers and Grades of Reagents and Enzymes

3-1: T_m values (with standard deviation) calculated from the thermal denaturation profiles of native and variant tRNA nucleotidyltransferases

3-2: Wavelength (\pm standard deviation) of fluorescence emission maximum of native or variant tRNA nucleotidyltransferases

3-3: Densitometry data from crude assays of tRNA nucleotidyltransferases

3-4: Summary of apparent kinetic parameters defined for native and variant tRNA nucleotidyltransferases when the tRNA concentration was varied

3-5: Summary of apparent kinetic parameters defined for native and variant tRNA nucleotidyltransferases when the CTP concentration was varied

3-6: Summary of apparent kinetic parameters defined for native and variant tRNA nucleotidyltransferases when the ATP concentration was varied

3-7: Densitometry data from crude assays of tRNA nucleotidyltransferases using variable metal ions as cofactor

3-8: Dissociation constants for ATP or CTP using the native or R64W enzymes

7-1: List of concentrations of native and variant tRNA nucleotidyltransferases determined using Bradford assay

LIST OF ABBREVIATIONS

AMP	Adenosine monophosphate
APS	Ammonium persulfate
ATP	Adenosine triphosphate
BSA	Bovine serum albumin
CCA	Cytidine-cytidine-adenosine
cDNA	Complementary deoxyribonucleic acid
CD	Circular dichroism
CMP	Cytidine monophosphate
CTP	Cytidine triphosphate
DNA	Deoxyribonucleic acid
dNTP	Deoxynucleoside triphosphate
EDTA	Ethylenediaminetetraacetic acid
Gdn-HCl	Guanidine Hydrochloride
GST	Glutathione-S-transferase
GTP	Guanosine triphosphate
IPTG	Isopropyl β -D-1-thiogalactopyranoside
K_m	Michaelis-Menten constant
k_{cat}	Turnover number
kDa	Kilodaltons
NTP	Nucleoside triphosphate
OD	Optical density
PAGE	Polyacrylamide gel electrophoresis
PBS	Phosphate buffered saline
PDB	Protein data bank
RNA	Ribonucleic acid

SDS	Sodium dodecyl sulfate
TBE	Tris borate EDTA buffer
TEMED	Tetraethylmethylenediamine
T_m	Melting temperature
tRNA	Transfer ribonucleic acid
tRNA-NT	Transfer ribonucleic acid nucleotidyltransferase
UTP	Uridine triphosphate
YT	Yeast extract, tryptone

1.0 INTRODUCTION

The enzyme, ATP(CTP):tRNA-specific tRNA nucleotidyltransferase (tRNA-NT), also commonly referred to as the CCA-adding enzyme, adds cytidine-cytidine-adenosine (CCA) to the 3'-ends of transfer RNAs (tRNAs) during their maturation (Morris and Herbert, 1970). This step is required for aminoacylation of the tRNA before it can serve its role in protein synthesis. The nucleotidyltransferase superfamily contains two classes of enzymes: Class I and Class II (Yue *et al.*, 1996). Phylogenetic studies suggest that the two classes of enzymes may have diverged very early in evolution (Xiong *et al.*, 2003). While class I enzymes share sequence similarity only at their active sites (Xiong *et al.*, 2003), class II nucleotidyltransferases, including eukaryotic and eubacterial CCA-adding enzymes, have maintained sequence conservation over much of their amino terminal regions (Li *et al.*, 2002).

1.1 Conserved motifs of Class II tRNA nucleotidyltransferases

Crystal structures for one eukaryotic (Augustin *et al.*, 2003; Kuhn *et al.*, 2015) and three eubacterial (Li *et al.*, 2002; Tomita *et al.*, 2004; Toh *et al.*, 2009;) CCA-adding enzymes have been solved. Based on these structures, tRNA nucleotidyltransferases have been compared to a seahorse consisting of four domains (Fig. 1-1): head, neck, body and tail (Li *et al.*, 2002). The active site of the enzyme is located in the head region while the other regions are also related to direct or indirect binding to incoming NTP or tRNA itself (Li *et al.*, 2002). The available crystal structures (Li *et al.*, 2002; Tomita *et al.*, 2004; Toh *et al.*, 2009; Kuhn *et al.*, 2015) show that the enzyme consists primarily of α -helices with only one β -sheet near the active site (Fig. 1-1). While the C-terminal portions of tRNA nucleotidyltransferases are not well conserved, the N-termini contain five conserved motifs that have been shown to play roles in substrate binding, organization and catalysis (Li *et al.*, 2002; Xiong *et al.*, 2003; Cho *et al.*, 2007). These motifs (A-E) are conserved in position and amino acid content (Fig. 1-2) and play a major role in defining the active site in tRNA nucleotidyltransferases (Fig. 1-3).

In the last 15 years, much research has gone into elucidating the roles of these conserved motifs and specific functions have been defined or attributed to each.

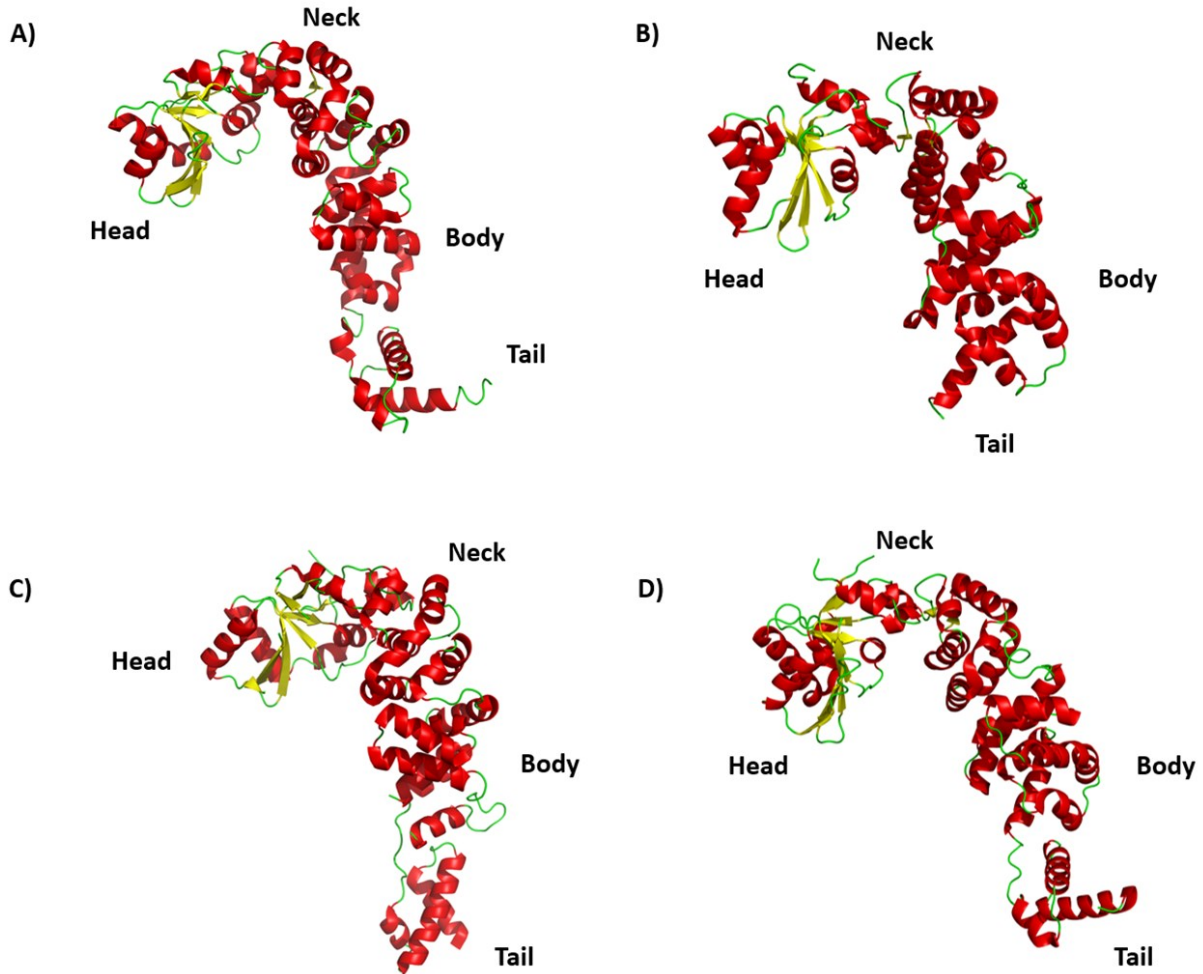


Figure 1-1: Crystal structures of class II tRNA nucleotidyltransferases. PyMol (Schrödinger) visualizations of tRNA nucleotidyltransferases (A) *Bacillus stearothermophilus* (PDB: 1MIV) (Li *et al.*, 2002) (B) *Aquifex aeolicus* (PDB: 1VFG) (Tomita *et al.*, 2004) (C) *Thermotoga maritima* (PDB: 3H37) (Toh *et al.*, 2009) (D) *Homo sapiens* (PDB: 4X4W) (Kuhn *et al.*, 2015). These structures show high α -helical content (red) and a common β -sheet (yellow) in the head domain with these secondary structures connected by loops/ β -turns (light green).

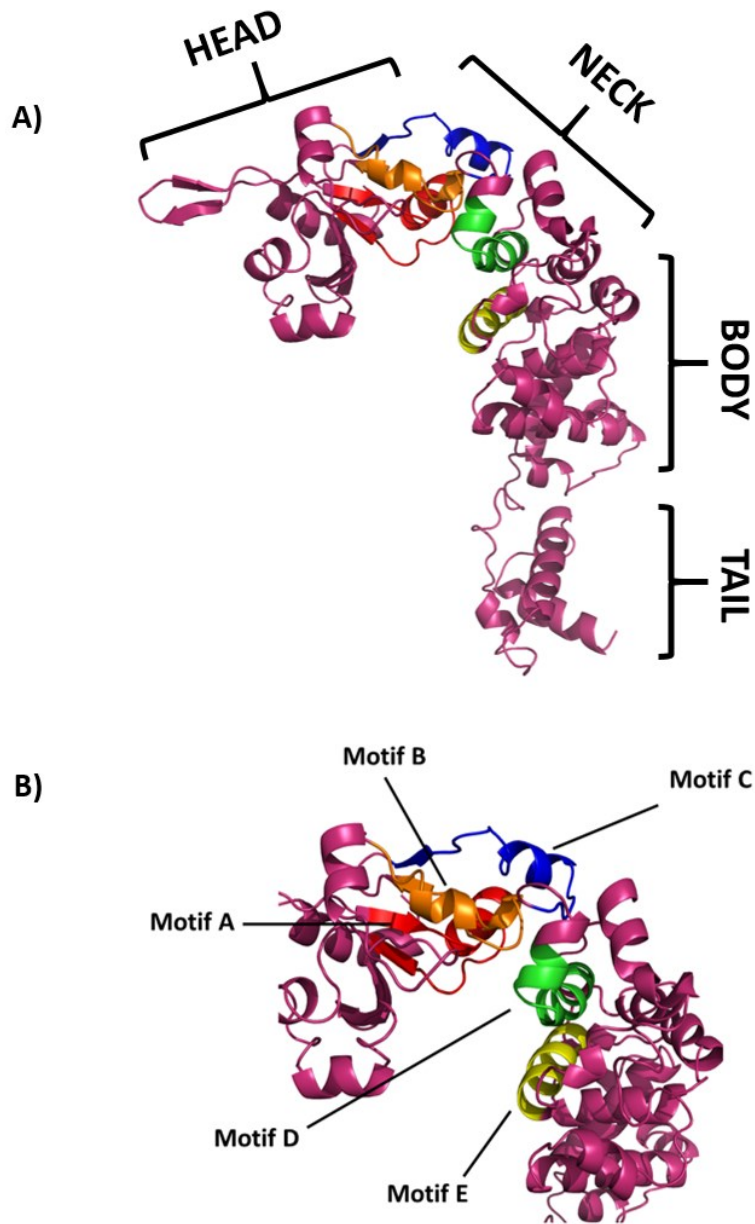


Figure 1-3: Model of *Saccharomyces cerevisiae* tRNA nucleotidyltransferase. This model was generated using the Phyre2 homology modeling server (Kelly *et al.*, 2015) and the representation was generated using PyMOL (Schrödinger). (A) The head, neck, body and tail regions are highlighted showing the seahorse structure characteristic of all tRNA nucleotidyltransferases. The conserved N-terminal motifs between the head and neck domains are also color coded: Motif A (red), Motif B (orange), Motif C (blue), Motif D (green) and Motif E (yellow); the rest of the protein is in magenta. (B) An enlargement of the conserved N-terminal portion of the protein with the conserved motifs indicated on the structure.

1.1.1 Motif A

Motif A contains two conserved aspartic acid residues which are thought to play a role in coordinating two magnesium cations that serve as cofactors in binding the triphosphate portions of the incoming nucleotide triphosphates (Steitz, 1998) assisting their addition to the bound tRNA (Fig. 1-4). Site-directed mutagenesis experiments have revealed the essential role of these two acidic amino acids (Xiong *et al.*, 2003, Steitz 1998). For example, conversion of either aspartic acid to alanine resulted in cell death in *Candida glabrata* and even the minor change from an aspartic acid to a glutamic acid was sufficient to make these yeast cells non-viable (Hanic-Joyce and Joyce, 2002).

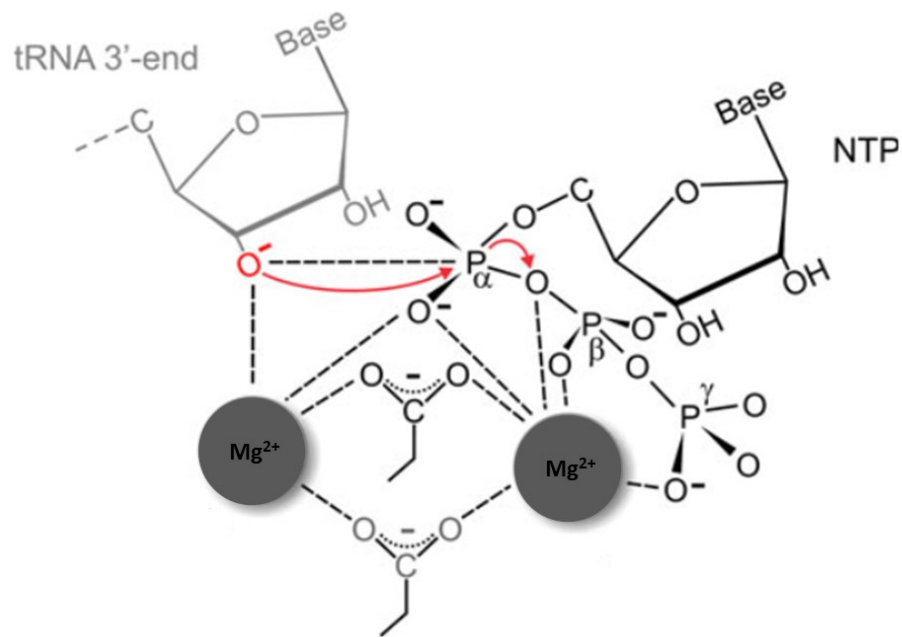


Figure 1-4: Reaction scheme for addition at motif A of a nucleoside triphosphate to a tRNA (Betat *et al.*, 2010; modified from Steitz, 1998). This is a common scheme by which nucleotide bases are added by all polymerases. The two Mg²⁺ ions are coordinated by the catalytically conserved carboxylates. The activated 3'-O⁻ (in red) in the 3'-OH group found in the tRNA primer (in grey) attacks the α-phosphate of the incoming nucleotide (red arrows). The Mg²⁺ ion (shown on the right) is thought to stabilize the triphosphate moiety of the NTP and facilitate the exit of the pyrophosphate group.

1.1.2 Motif B

Motif B is thought to play a role in discriminating between ribonucleotides and deoxyribonucleotides by allowing a hydrogen bond to form between the 2'-OH of the ribose of the incoming nucleotide triphosphate and the guanidium side chain of the central arginine in the conserved RRD sequence (Li *et al.*, 2002). The deoxyribonucleotides, lacking the 2'-OH group, cannot form this hydrogen bond. Again, site-directed mutagenesis has been used to show the importance of these residues, as replacing the central arginine residue with a glutamate or glutamine in the *Bacillus stearothermophilus* tRNA-NT leads to the inability of motif B to distinguish between ribonucleotides and deoxyribonucleotides (Cho *et al.*, 2007). More recently, naturally occurring mutations leading to disease phenotypes in humans have been mapped to the region of the TRNT1 gene coding for this motif (Chakraborty *et al.*, 2014; Sasarman *et al.*, 2015). These results indicate that the role of this motif has been conserved from bacteria to eukaryotes.

1.1.3 Motif C

Motif C is the least well characterized of all the conserved motifs. Among the five sequences compared in Fig. 1-2, only two amino acid positions (glycine 195 and arginine 205) are absolutely conserved. Due to its overall lower sequence similarity among class II nucleotidyltransferases, it was historically believed to function simply as a link between the head and neck domains (Li *et al.*, 2002; Cho *et al.*, 2007). However, recent studies have indicated that motif C may actually have a role in function. We initially identified a mutation changing the glutamic acid at position 189 in motif C of the yeast enzyme to a lysine that resulted in a temperature-sensitive phenotype (Shan *et al.*, 2008). Conversion of position 189 in the yeast enzyme to lysine or phenylalanine also resulted in cell death at the restrictive temperature (Fig. 1-5).

We initially showed that this substitution resulted in a structural change in the protein that reduced enzyme activity (both at the permissive and restrictive temperatures), decreased the melting temperature of the protein and altered its stability at the restrictive temperature (Shan *et al.*, 2008). Subsequently, we showed that a second site mutation in motif A (R64W) restored

activity and suppressed the temperature-sensitive phenotype (Fig. 1-5) suggesting for the first time a novel relationship between motifs A and C in tRNA nucleotidyltransferase (Goring *et al.*, 2013).

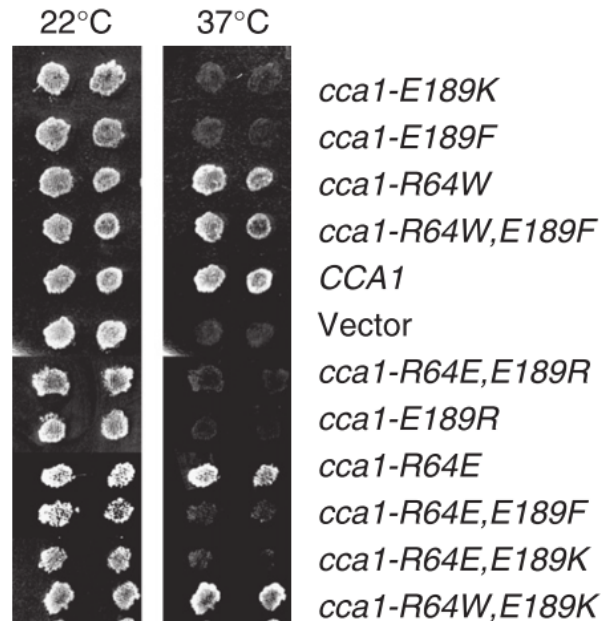


Figure 1-5: Replica plating results to identify temperature-sensitive mutants of the *CCA1* gene (Goring *et al.*, 2013). The yeast growth was monitored from two individual transformants in SC medium lacking uracil while incubating at 22°C (permissive) and 37°C (restrictive) temperatures to assess temperature sensitivity. The figure indicates the temperature-sensitive mutants E189K, E189R and E189F, the double mutant suppressors R64WE189F and R64WE189K, the single variants R64W and R64E, and the vector alone. In addition, double mutants involving R64E in the form of R64EE189F and R64EE189K, were also monitored to show the significance of R64W in suppressing the temperature-sensitive phenotype.

In that same study, variant proteins were generated which contained an R64W substitution alone or in combination with E189F (R64WE189F). As illustrated in Fig. 1-6, the R64W substitution by itself did not eliminate enzyme activity indicating that an arginine was not required at position 64 (Goring *et al.*, 2013). More interestingly, the introduction of this second substitution (R64W) to the E189F variant restored activity greatly (although not to the level of the native enzyme) at both the permissive and restrictive temperatures (Goring *et al.*, 2013).

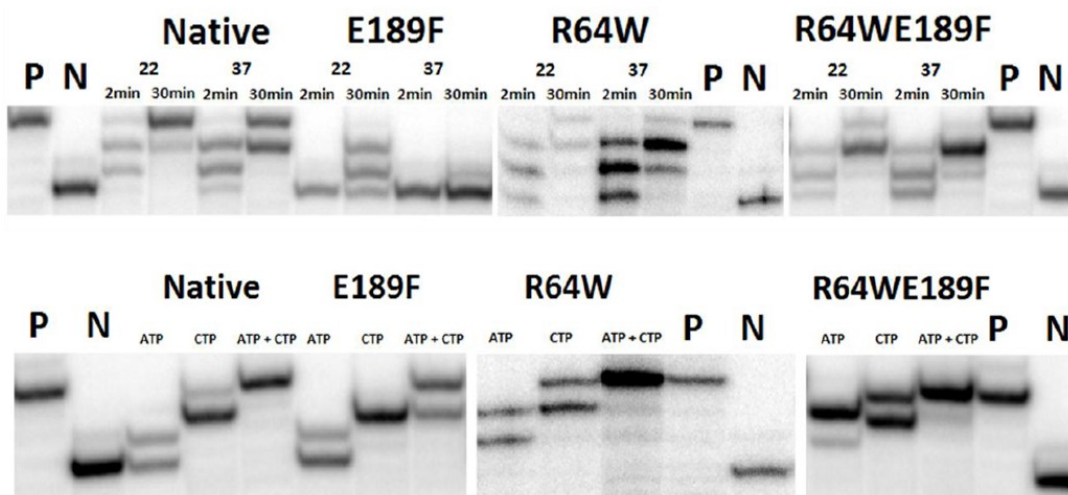


Figure 1-6: Nucleotide addition by tRNA nucleotidyltransferase variants (Goring *et al.*, 2013). (A) The enzymes (5 ng) were incubated with a tRNA-N transcript for 2 or 30 min at 22°C or 37°C, and the products separated by polyacrylamide gel electrophoresis. P, positive control (active enzyme generating a product containing a complete CCA sequence), N, negative control (boiled enzyme leaving a product lacking the CCA sequence). (B) The reactions were allowed to go to completion at 22°C with the tRNA-N transcript and the nucleotides indicated; and the products separated by polyacrylamide gel electrophoresis.

The study also detected a difference in the ability to discriminate between ATP and CTP as nucleotide triphosphate substrates (Fig. 1.6). While the native enzyme and the E189F variant could incorporate AMP instead of CMP at the first position with limited efficiency, adding the R64W change to either enzyme increased misincorporation of AMP at both the first and second positions. With respect to CMP incorporation, the E189F variant showed little or no CMP misincorporation at the third position while the native enzyme showed a small amount of CMP incorporation at this position and both of the R64W variants (R64W and R64WE189F) showed a high level of CMP incorporation at the third position. Taken together these data suggest that somehow the change of R64 to tryptophan results in a loss in substrate specificity perhaps by altering the arrangement of amino acids at the active site. They also confirm what we had shown previously (Shan *et al.*, 2008) that the E189F substitution reduces enzyme activity suggesting that this substitution also alters the arrangement of residues in the active site region. Moreover, the

R64W substitution while increasing the chances of misincorporation of amino acids also increases catalytic activity in the poorly active E189 variants.

In addition to our data suggesting that the E189F mutation alters the arrangement of amino acids at the active site to reduce activity, Ernst *et al.* (2015) suggest that motif C acts as a flexible spring providing the proper orientation of the head and neck domains to accommodate the growing 3'-OH end of the tRNA substrate. They showed that converting the highly conserved aspartic acid residue (corresponding to position 190 in the yeast enzyme and adjacent to the glutamic acid residue that we had explored at position 189) interferes with AMP incorporation and affects interdomain movements in the enzyme. They propose that these conformational transitions are involved in the switch in specificity of the nucleotide-binding pocket from CTP to ATP during CCA-synthesis (Fig. 1-7).

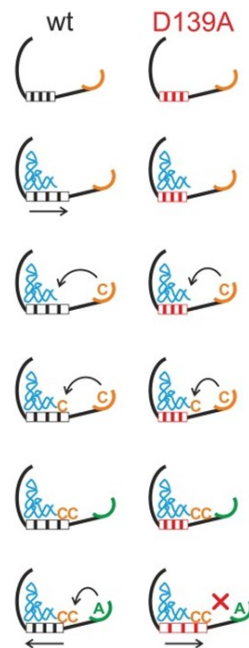


Figure 1-7: Mechanistic model for different motif C states during CCA-addition (Ernst *et al.*, 2015). Motif C shown as striped portion (black indicates proper spring motion upon growth of 3' end of tRNA in native enzyme; while red shows inability do so in the D139A variant).

Taken together, our results targeting amino acid 189 in the yeast enzyme as well as the results of others who targeted the adjacent amino acid in the human enzyme reveal that motif C plays a role in enzyme activity and suggest that this domain may interact with other domains in tRNA nucleotidyltransferase.

1.1.4 Motif D

Motif D helps recognize sequentially the incoming CTP, CTP and ATP nucleotide triphosphates (Fig. 1-8) and to discriminate against GTP and UTP. Three conserved residues (glutamate, aspartate and arginine) in motif D form Watson-Crick like hydrogen bonds with incoming NTPs (Cho *et al.*, 2007; Li *et al.*, 2002). The addition of the first two CTPs is followed by reorganization of this region of the enzyme such that specificity is adjusted from CTP recognition to ATP recognition, hence completing full CCA addition (Li *et al.*, 2002). Site-directed mutagenesis in the *B. stearothermophilus* tRNA nucleotidyltransferase, converting the conserved Glu153, Asp154 and Arg157 residues to Asn/Ser, Glu and Asn, respectively, resulted in the conversion of a CCA-adding enzyme to a UUG-adding enzyme (Cho *et al.*, 2007) highlighting the importance of these residues in nucleotide recognition. Interestingly, in *A. aeolicus* which has separate CC- and A-adding enzymes, motif D in the CC-adding enzyme has an arginine instead of the conserved glutamate, resulting in the inability of ATP to be added by this enzyme (Li *et al.*, 2002). In the *C. glabrata* enzyme we showed that the conserved arginine (analogous to R157 in Fig. 1-8) limits the binding pocket size and orients active site Asp and Arg residues to discriminate against AMP addition at the first position; thus supporting the role of motif D to incorporation efficiency and nucleotide specificity (Colasurdo, 2011).

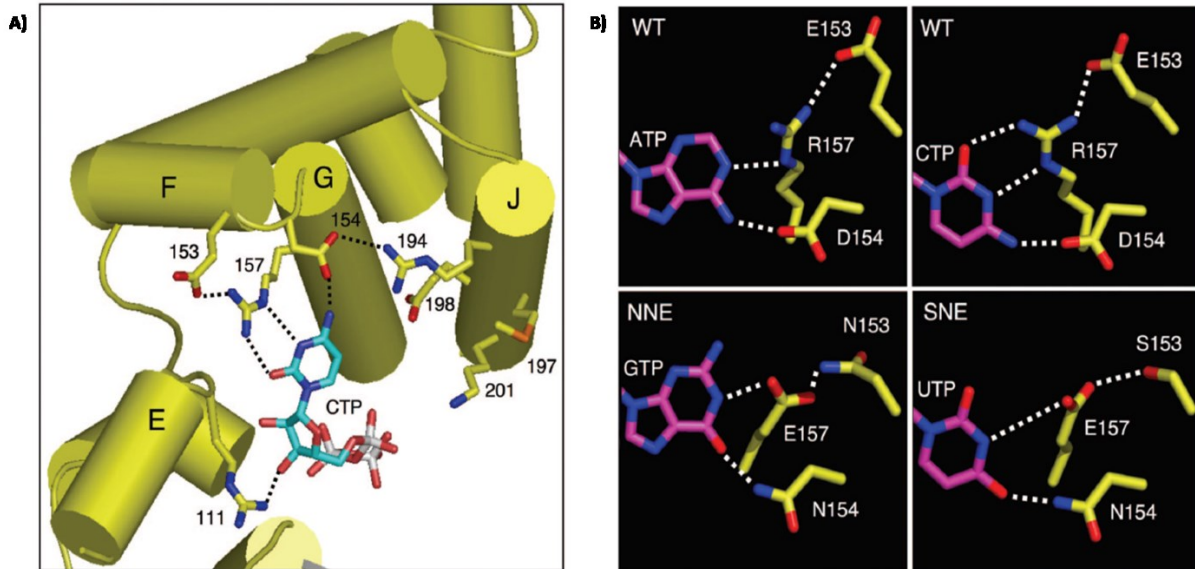


Figure 1-8: Interactions between the *Bacillus stearothermophilus* CCA-adding enzyme and tRNA (Cho *et al.*, 2007). (A) Nucleotide binding site in *B. stearothermophilus* CCA-adding enzyme composed of the head and neck domains where catalytic R111 (in Motif B) interacts with the 2'-OH of ribose of CTP (substrate). In the stick representation: N (blue), O (red), C (yellow in polypeptide; light blue in the nucleotide); and H-bonds (black dashed lines). (B) Watson-Crick-like interactions of ATP or CTP (top) with the *B. stearothermophilus* CCA-adding enzyme, and with GTP or UTP (below) when the binding site was redesigned Cho *et al.* (2007). The stick representation is similar to (A), except C (purple) and H-bonds (white dashed lines).

1.1.5 Motif E

Similar to motif C, researchers have been unable to establish a complete understanding of the role of motif E. However, some studies have indicated that it may have a role in stabilizing the secondary structure of motif D by directly interacting with mature tRNA (Cho *et al.*, 2007; Li *et al.*, 2002). We previously studied the arginine residue at position 244 in *C. glabrata* tRNA nucleotidyltransferase (corresponding to R194 in Fig. 1-8), which supported the idea that motif E may be responsible for recognizing the nucleotide triphosphate substrate and hence facilitate the switch from CTP to ATP (Arthur, 2009). This amino acid may also play a role in the orientation of the growing the 3' end of tRNA to limiting nucleotide addition to three bases (Arthur, 2009).

1.1.6 The carboxy-terminal body and tail domains

There are no obvious sequence conservations in the carboxy-terminal portion of the protein containing the body and tail domains. These domains have been proposed to have a role in anchoring the tRNA substrate (Betat *et al.*, 2004), by interacting with the sugar-phosphate backbone and some portions of the anticodon and TΨC loops of the tRNA structure (Betat *et al.*, 2010). We have shown that amino acid substitutions in this region of the Arabidopsis protein can alter the stability of the protein and influence its intracellular distribution (Leibovitch *et al.*, 2013) suggesting that this portion of the protein may play a role in protein targeting. Others have shown that the carboxy-terminal portion of the *E. coli* tRNA nucleotidyltransferase exhibited Ni²⁺ dependent phosphatase activity, a metal-independent 2', 3'-cyclic activity and a 2'-nucleotidase phosphodiesterase activity linked to RNA repair at the 3' end of tRNA (Yakunin *et al.*, 2004). Thus, this portion of the enzyme may play different roles in different organisms.

1.2 Project Objectives

The primary objective of this study was to establish a better understanding of the role of motif C in tRNA nucleotidyltransferase activity. Our previous findings in *S. cerevisiae* (Shan *et al.*, 2008, Goring *et al.*, 2013) and a recent study with the human homologue (Ernst *et al.* 2015) have argued for a role of motif C in tRNA nucleotidyltransferase both in active site organization and reorganization during catalysis. Our studies used genetic, biophysical and biochemical approaches to explore the role of a glutamic acid residue at position 189 of the yeast enzyme while Ernst *et al.* (2015) used modeling, EPR and biochemical data to explore the role of a conserved aspartic acid at position 139 in the human tRNA nucleotidyltransferase (analogous to aspartate 190 in yeast). Both studies showed the importance of these adjacent acidic amino acids and by extension motif C in the function of tRNA nucleotidyltransferase. Moreover, Ernst *et al.* (2015) suggest a role for this motif in the rearrangement of the active site of the enzyme during catalysis, which is in good agreement with our observations (Goring *et al.*, 2013) that structural changes in motif C may be linked to motif A. Therefore, both glutamate 189 and aspartate 190 were investigated in the *S. cerevisiae* tRNA nucleotidyltransferase to develop a better understanding of their roles in enzyme structure and function. The secondary objective of this study was to understand the role of arginine 64 in the function of motif A and to explore how motifs A and C may interact such that changing arginine 64 to tryptophan in motif A causes suppression of the temperature-sensitive phenotype resulting from changes in motif C.

To address these questions, a number of variant proteins (R64W, D190A, D190F, R64WD190A, R64WD190F, E189A, R64WE189A and E189Q) with amino acid substitutions in motifs C and/or A were generated and characterized biochemically and biophysically. Spectroscopic techniques (circular dichroism and fluorescence) and proteolysis experiments were used to assess changes in higher order structure, thermal stability, and dissociation constants (K_d) while *in vitro* enzyme assays were used to see how these substitutions affects the kinetic parameters of the yeast tRNA nucleotidyltransferase.

2.0 MATERIALS AND METHODS

2.1 Strains, Buffers, Growth Media, and Solutions

Table 2-1 includes a list of buffers, solutions and growth media used in this study, as well as the reagents required to prepare them. Table 2-2 indicates the grade and manufacturer of reagents and enzymes used.

Table 2-1: Components for Buffers, Solutions and Growth Media

Buffers, Growth Media, and Solutions	Required Components
30% Acrylamide Solution (29:1) (Sambrook <i>et al.</i> , 1989)	29 g acrylamide, 1 g <i>bis</i> -acrylamide; fill to 100 mL in dH ₂ O and store at 4°C in the dark
40% Acrylamide Solution (19:1) (Bio-Rad Laboratories, 1995)	38 g acrylamide, 2 g <i>bis</i> -acrylamide; fill to 100 mL with dH ₂ O and store at 4 °C in the dark
Elution Buffer (pH: 7.8) (Colasurdo, 2011)	15 mM glutathione in 1X PBS adjusted to pH 8.3 with HCl
PBS (1X) (pH 7.45) (Sambrook <i>et al.</i> , 1989)	8 g (137 mM) NaCl, 0.2 g (2.7 mM) KCl, 2.68 (10 mM) Na ₂ HPO ₄ , 0.25 g (1.8 mM) KH ₂ PO ₄ ; fill to 1 L with dH ₂ O and store at 4 °C, adjusted pH with HCl
Peattie's Loading Dye (100 mL) (Peattie, 1979)	10 M urea, 5 mM Tris base/boric acid or Tris-borate (pH 8.3), 0.1 mM EDTA, 0.05% xylene cyanol, 0.05% bromophenol blue
Resuspension Buffer (Colasurdo, 2011)	1X PBS (pH 7.4), 1 mM EDTA
SDS (5X) Loading Dye (Modified from Walker, 2002)	45 mM Tris-HCl (pH 6.8), 10% SDS (w/v), 50% glycerol (v/v), 25% β-mercaptoethanol (v/v), 0.25% bromophenol blue (w/v)
SDS (5X) Running Buffer (1 L) (Modified from Sambrook <i>et al.</i> , 1989)	72 g (1 M) glycine, 15 g (1 M) Tris-HCl, 5 g (17 mM) SDS, dH ₂ O to one litre

Buffers, Growth Media, and Solutions	Required Components
SDS Staining Solution A (Wong <i>et al.</i> , 2000)	25% isopropanol, 10% acetic acid, 0.05% Coomassie brilliant blue
SDS Destaining Solution B (Wong <i>et al.</i> , 2000)	10% isopropanol, 10% acetic acid, 0.005% Coomassie brilliant blue
SDS Destaining Solution D (Wong <i>et al.</i> , 2000)	10% isopropanol, 10% acetic acid
SDS-PAGE Resolving Gel (10 ml) (Modified from Sambrook <i>et al.</i> , 1989)	4.3 mL 30% acrylamide solution, 3 mL dH ₂ O, 2.5 mL 1.5 M Tris-HCl (pH 8.8), 100 µL 10% SDS, 100 µL 10% APS, 10 µL TEMED
SDS-PAGE Stacking Gel (10 ml) (Modified from Sambrook <i>et al.</i> , 1989)	1.4 mL 30% acrylamide solution, 6.0 mL dH ₂ O, 2.5 mL 0.5 M Tris-HCl (pH 6.8), 100 µL 10% SDS, 100 µL 10% APS, 10 µL TEMED
TBE (5X) (1 L) (Modified from Sambrook <i>et al.</i> , 1989)	30 g (250 mM) Tris, 15.5 g (25 mM) boric acid, 10 mL 0.5 M EDTA (5 mM, pH 8.0), dH ₂ O to one liter
7M Urea, 12% Polyacrylamide Gel (~100 ml) or (~10 ml for mini-gel) (Bio-Rad Laboratories, 1995)	30 mL 40% acrylamide solution, 42 g (7 M) urea, 20 mL 5X TBE, 20mL dH ₂ O; 100 µL 25% APS and 100 µL TEMED; For the mini gel, one-tenth volume of the reagents are used
YT (Sambrook <i>et al.</i> , 1989)	0.5% Yeast extract, 0.8% Tryptone, 0.5% NaCl

Table 2-2: Suppliers and Grades of Reagents and Enzymes

Chemical/Reagent	Grade	Supplier
Acrylamide	Ultra pure	Bioshop
Acetic acid	ACS	Caledon
Adenosine triphosphate (ATP) [α - ³² P] (10 μ Ci/ μ L, 3000 Ci/mmol)		Perkin Elmer
Agar	Bacteriological Grade II	Bioshop
Agarose	Electrophoresis Grade	Bioshop
Alkaline Phosphatase (Calf)		New England Biolabs
Alpha-Chymotrypsin (pancreatic)		Sigma Aldrich
Ammonium acetate	ACS	Omega
Ammonium persulfate (APS)		Bioshop
Ampicillin (AMP)		Goldbio
Baker's yeast tRNA	Crude	Roche
<i>Bam</i> HI (restriction enzyme)		New England Biolabs
β -mercaptoethanol		ICN
<i>Bis</i> -acrylamide	BioUltra pure	Bioshop
Boric acid	Biotechnology Grade	Bioshop
<i>Bpi</i> I (restriction enzyme)		New England Biolabs
Bromophenol blue	Electrophoresis Grade	Bio-Rad
<i>Bst</i> I (restriction enzyme)		Promega
Calcium chloride (dihydrate)	Molecular Biology Grade	Bioshop
Coomassie Brilliant Blue	BioUltra pure	Bioshop
D-Lactose (monohydrate)		Bioshop
EDTA (Disodium salt)	Biotechnology Grade	Bioshop
Ethanol		Commercial Alcohols Inc.
Ethidium Bromide		Sigma-Aldrich

Chemical/Reagent	Grade	Supplier
<i>FokI</i> (restriction enzyme)		New England Biolabs
GeneJet Plasmid Miniprep kit		Fermentas
Glutathione (reduced)	High purity Grade	Bioshop
Glutathione Sepharose 4 Fast Flow		Goldbio
Glycerol	Molecular Biology Grade	Fisher
Glycine	Biotechnology Grade	Bioshop
Guanidine Hydrochloride	Biotechnology Grade	Bioshop
Hydrochloric acid	ACS	Caledon
Isopropanol		Fisher
Isopropyl- β -D-thiogalactopyranoside (IPTG)		Goldbio
Magnesium acetate	ACS	Anachemia
Magnesium chloride hexahydrate	Biotechnology Grade	Bioshop
Nucleotide triphosphates		Fermentas
Nuclease Free dH ₂ O	Dnase/Rnase Free	Bioshop
PerfectPrep Plasmid XL kit		Fisher
Phenol	Molecular Biology Grade	Fisher
Potassium chloride		BDH
Potassium phosphate (monobasic)	ACS	Anachemia
RNase A (pancreatic)		Bioshop
RNAsecure Reagent		Ambion
<i>Sall</i>		Clontech
Snake venom phosphodiesterase		Sigma-Aldrich
Sodium acetate	Enzyme Grade	Fisher
Sodium chloride	ACS	Fisher
Sodium dodecyl sulphate (SDS)	Ultra pure	Bioshop
Sodium hydroxide		Fisher

Chemical/Reagent	Grade	Supplier
Sodium phosphate heptahydrate (dibasic)	ACS	Bioshop
Tetramethylethylenediamine (TEMED)	Ultra pure	Biobasic Inc
T4 DNA ligase		New England Biolabs
T7 RNA polymerase		Fermentas
Thrombin (1 U/ μ L)		GE Healthcare
Tris	BioUltra pure	Bioshop
Tryptone	Bacteriological Grade	Bioshop
Urea		A & C (American Chemicals)
Xylene cyanol	Electrophoresis Grade	Fisher
Yeast Extract		Bioshop

2.2 Construction of Expression System

Quikchange (Stratagene) mutagenesis (Liu and Naismith, 2008) was performed using *Pfu* (Thermo, 2.5 U/ μ L) polymerase-mediated amplification of plasmid templates pGEX2T-SCR9-1 or SCR9-1 (Goring *et al.*, 2013). The plasmid SCR9-1 and its derivatives were provided by Matthew Leibovitch, Mark Goring and Pamela Hanic-Joyce. The plasmid sequences were confirmed by sequence analysis (McGill University and Genome Quebec Innovation Centre).

2.3 Expression and purification of yeast tRNA nucleotidyltransferase proteins

2.3.1 Protein Expression (modified from Shan *et al.*, 2008)

E. coli BL21 (DE3) cells (50 μ L from an overnight culture of cells from -80°C or single colonies scraped from a fresh plate) containing the plasmids of interest were inoculated into 10 mL YT with 100 $\mu\text{g}/\text{mL}$ ampicillin and grown overnight (16-18 hours) at 37°C in a Lab-line Orbital shaker at 225 rpm. These 10 mL cell cultures were divided into two 5 mL aliquots and transferred to two Fernbach flasks, each containing 1.3 L of YT medium and ampicillin (100 $\mu\text{g}/\text{mL}$). The cultures were incubated in a New Brunswick Scientific Innova 4330 Refrigerated Incubator Shaker at 37°C and 225 rpm until the OD_{600} reached between 0.4-0.6 (typically 2-3 hours). After that, the cells were induced with a final concentration of 0.02% D-lactose and 0.5 mM IPTG and returned to the shaker at 19°C and 225 rpm for another 16-20 hours. When protein expression was low, the IPTG concentration and temperature were lowered to 0.2 mM and 16°C , respectively and the incubation time was increased to 48 hours. Using a Beckman JA-10 rotor, the cells were pelleted at 4°C by centrifuging for 15 minutes at 6 000 rpm. The supernatant fluid was discarded and the pellets were stored at -80°C and frozen for at least an hour before use.

2.3.2 Cell Lysis (modified from Shan *et al.*, 2008)

The frozen cell pellets were placed on ice to thaw and resuspended by vortexing (30 sec vortexing followed by 30 sec on ice, repeated 10 times) in 2 mL cold lysis buffer (1X PBS and 1 mM EDTA) for every gram of cell pellet. This solution was passed through a French Pressure cell (Thermospectonic) 3-4 times at 1 000 psi and the resulting cell lysate was centrifuged at 18 000 rpm in the Beckman JA-20 rotor for 30 minutes at 4°C . The supernatant was transferred to a new tube and the centrifugation repeated. This step removes cell debris and the resulting cleared supernatant was used for column chromatography.

2.3.3 GST-tagged affinity column (Harper *et al.*, 2011)

A Glutathione Fast Flow 4B chromatography resin (GE Healthcare) was used for the purification of GST-tagged tRNA nucleotidyltransferase. About 2-3 mL of this resin was packed in a 1.5 cm x 10 cm Bio-Rad column. About 10 bed volumes of 1X PBS (pH 7.45) were passed through the column to equilibrate it. At the end of each round of purification, the resin was regenerated by washing the resin with 5 mL of 6M guanidine-HCl, about 50 mL of distilled water and then 70% ethanol. The column was stored in 20% ethanol at 4°C.

2.3.4 Purification, thrombin cleavage and dialysis (modified from Shan *et al.*, 2008)

The supernatant, after cell lysis, was cycled through the Glutathione Fast Flow 4B column overnight at 4°C at a flow rate of approximately 1 mL/min using a pump (VWR). The following day, the lysis buffer was collected and the column washed first with 300-500 mL of 1X PBS (flow rate of 3 mL/min) to eliminate non-specific binding. Subsequently, protein was eluted from the column with 20 mL of elution buffer (15 mM reduced glutathione in 1X PBS) and collected as 1 mL fractions. The resulting fractions were analyzed using SDS-PAGE to screen for protein content and the appropriate fractions containing the protein of interest were pooled. This step was followed by dialysis of the pooled fractions (typically approximately 10 mL) using a 6-8 kDa pore size dialysis bag (Spectra/Por) with 50 units of thrombin added first. The dialysis is executed overnight against 5 L of 1X PBS at 4°C, with buffer changes at the 2 h and 4 h marks. The following day the protein solution was removed from the dialysis bag and 1.5 mL aliquots were centrifuged in microfuge tubes at 4 400 xg for 5 minutes at 4°C. This step removed protein aggregates which may have been generated during dialysis and which may eventually clog the Glutathione Fast Flow 4B column. In addition, an aliquot of each sample was checked by SDS-PAGE to ensure maximum thrombin cleavage was achieved.

The protein solution after dialysis and centrifugation was then cycled through a freshly regenerated Glutathione Fast Flow 4B column three times to remove the GST portion of the sample (either free GST or uncut GST+tRNA-NT fusion protein). The resulting eluent should be

pure tRNA-NT. To ensure that maximum purity was achieved the column was regenerated after the second pass. Even though this reduced the yield, the final sample was more pure with less contaminating GST or GST+tRNA-NT fusion protein. The resulting protein was stored in aliquots at -80°C after glycerol had been added to a final concentration of 10% (v/v).

2.3.5 Sodium dodecyl sulfate polyacrylamide gel electrophoresis (SDS-PAGE) (modified from Sambrook *et al.*, 1989)

The resolving gel (Table 2-1) was prepared and cast between two 4 cm by 10 cm glass plates separated by 0.75 mm spacers. About 3.5 mL of the resolving gel was poured between the plates. Once the resolving gel had polymerized, the stacking gel was added and the 10-well or 15-well (used for proteolysis experiment in section 2.7) comb inserted immediately. When the stacking gel had polymerized, the comb was removed and the samples loaded after being boiled for 2-5 minutes and then cooled on ice. The wells were rinsed with SDS running buffer (1X) to remove any residue before the samples were loaded. Electrophoresis was carried out at 200 V for about 1.5 hours or until the bromophenol blue dye front migrated off the gel. The gel was stained and destained to visualize pure protein (Wong *et al.*, 2000). After staining, the gel was carefully washed with dH₂O and framed.

2.3.6 Protein Concentration determination

The protein sequences were analyzed using the ProtParam tool (Gasteiger *et al.*, 2005) to predict the molar extinction coefficient (ϵ) which was found to be 50100 M⁻¹cm⁻¹ for the short native enzyme at 280 nm (assuming that all of the cysteines are reduced). It also allowed the prediction of the molecular weight to be 60 638 Da. Using the Cary 100 Bio UV-Visible Spectrophotometer and 1.0 cm quartz cell, at a wavelength of 280 nm, the absorption of the protein was recorded, and using the Beer-Lambert law, the concentration was calculated. Since the protein samples typically contained *E. coli* tRNA from the purification procedure, the samples were RNase A (Bioshop) treated by addition of 30 ng/mL of RNase A with incubation for 1 hour at room temperature. The sample was dialyzed again in 1X PBS as described above (Section 2.3.4) to remove any free nucleotides generated and the loss of nucleic acid confirmed by UV/Vis

Spectroscopy. Protein concentrations also were determined by Bradford Assay (Bradford, 1976) using bovine serum albumen (Sigma-Aldrich) and the Bradford reagent (Bio-Rad) and the protocol recommended by the supplier.

2.4 Biophysical Characterization of yeast tRNA nucleotidyltransferase

2.4.1 Circular Dichroism Spectroscopy

2.4.1.1 Secondary Structure Analysis (Peptide Backbone Scans)

The procedure of Leibovitch *et al.* (2013) was followed except that the scans were taken between 200-260 nm. A Jasco-815 Circular Dichroism Spectrophotometer with “Spectral Management” program software (Jasco) was used for this analysis. The data were accumulated five times at 20°C for an aliquot of 400 µL of each protein. All of these proteins were RNase A treated as described in section 2.3.6 to avoid RNA interference. The samples were dialyzed extensively (for 16-20 hours) with 1X PBS and centrifuged at 4°C for 5 minutes at 4 400 xg. Before the CD spectra were obtained, the samples were checked using UV/Vis spectroscopy to ensure that any contaminating ribonucleotides had been removed. Spectra for each protein were smoothed using the smoothing function in the Spectra Analysis (Jasco) program.

2.4.1.2 Thermal Denaturation Profiles

Procedure taken from Leibovitch *et al.* (2013). The instrument and parameters used were the same as in section 2.4.1.1 except that the “Variable Temperature” program was used in the temperature range 20-80°C. The following formula was used to calculate the melting temperature $F = 1 / \Delta\theta T \times \theta - \theta_i / \Delta\theta T$, where F is the fraction of unfolded protein, θ is ellipticity (deviation in absorption of circularly polarized light) measured in mdeg, and $\Delta\theta T$ is the total change in ellipticity between the initial and final temperatures of interest; $\Delta\theta T = \theta_f - \theta_i$. θ_i is the ellipticity value at the start temperature of interest (20°C), and θ_f is the final ellipticity value at the end temperature.

2.4.2 Fluorescence Spectrophotometry

Procedure taken from Leibovitch *et al.* (2013). A Varian Cary Eclipse Fluorescence Spectrophotometer was used to record fluorescence emission spectra and the “Scan” application at 20°C collected 10 scans (CAT scans) between 310 nm and 400 nm. The excitation wavelength was set at 280 nm or 295 nm and the scan speed was set to medium (600 nm/min) with a 1.0 nm data sampling interval, 5 nm excitation and emission slit widths and voltage set to medium (600 V) with a 1.0 cm quartz cell.

2.4.3 Fluorescence Quenching of native and R64W proteins using ATP or CTP (modified from Shan *et al.*, 2008)

Fluorescence quenching experiments were done to determine the apparent dissociation constants (K_d) for ATP or CTP for the native and R64W proteins. The protein samples were RNase A treated (as explained in section 2.3.6) and extensively dialyzed in 1X PBS and centrifuged to avoid aggregates. Before the spectra were obtained, the samples were checked using UV/Vis spectroscopy to ensure that any contaminating ribonucleotides had been removed. An OD_{280} of approximately 0.075 was achieved for the proteins before carrying out these experiments. The setting and parameters used in Section 2.4.2 were used for these experiments. The formula used to calculate the degree of fluorescence quenching was $F_c = F_o \times (V_f/V_0) \times \text{antilog}[(OD_{ex} + OD_{em})/2]$, where F_c and F_o refer to the corrected and observed fluorescence, respectively, OD_{ex} and OD_{em} refer to the absorbance at the excitation and emission wavelengths, respectively, V_f and V_0 refer to the volume of the solution after the addition of ATP or CTP and the initial volume, respectively. Using $F_{c0}-F_{ci}/F_{c0}$ on the y-axis, it was plotted against ATP or CTP concentration leading to the K_d values, where F_{c0} is the corrected fluorescence in the absence of quencher and F_{ci} is the corrected fluorescence at each quencher concentration. The formula used by GraFit 7 is as follows: $F_{c0}-F_{ci}/F_{c0} = (F_{max} \cdot [ATP \text{ or } CTP]) / (K_d + [ATP \text{ or } CTP])$ where F_{max} is the constant that signifies no more quenching that occurs regardless of addition of more quenchers leaving the ratio of fluorescence unchanged.

One modification from the published protocol was that 7 μL of 1M MgCl_2 (final concentration 10 mM) was added to 693 μL of sample, because the quenching experiment did not work without the cofactor. To this 700 μL , small volumes (total volume of 730 μL when 150 μM is reached) of ATP and buffer or CTP and buffer were added to achieve final nucleotide triphosphate concentrations of 0.5 μM , 1 μM , 2 μM , 3 μM , 5 μM , 8 μM , 10 μM , 25 μM , 50 μM , 75 μM and when necessary 100 μM , 125 μM and 150 μM (until no more quenching was possible). At the same time, ultraviolet-visible spectral scans (200-400 nm) were recorded with same concentrations of ATP or CTP, except in 1X PBS with no protein to take into account the inner-filter effect (reabsorption of light by the quencher). The fluorescence excitation wavelength was 290 nm and 330 nm was taken as the fluorescence emission maximum.

2.5 Enzyme Activity Assays

2.5.1 Run-off transcription and purification of transcripts

For preparation of the tRNA transcripts, the procedure was followed as per Leibovitch *et al.* (2013) and the restriction digestions were carried out on plasmids G73 (using *FokI*) and pmBsDCCA (using *FokI*, *BpiI* or *BstOI*) to generate linearized templates to produce tRNA-N, tRNA-NC (C74), tRNA-NCC (C75) and tRNA-NCCA (A76) run-off products, respectively. The products were purified by phenol extraction and ethanol precipitation (Sambrook *et al.*, 1989).

Run-off transcription was performed as per the protocol in Leibovitch *et al.* (2013), using T7 RNA polymerase and the appropriate linearized template. Each run-off transcription reaction contained 20 μL 5X transcription buffer, 5 μL of 1 mM ATP, 5 μL 10 mM CTP, 5 μL 10 mM UTP, 5 μL 10 mM GTP, approximately 50 μCi ($\sim 5 \mu\text{L}$) [α - ^{32}P] ATP (10 $\mu\text{Ci}/\mu\text{L}$, 3000 Ci/mmol), $\sim 10 \mu\text{g}$ of linearized DNA template, 3 μL of T7 RNA polymerase (60U) and nuclease-free water to 100 μL . The reaction was incubated for 2-3 hours at 37°C and terminated via phenol extraction followed by ethanol precipitation. The resulting pellet was resuspended in 10 μL nuclease-free water and 10 μL of Peattie's (2X) loading dye was added. After heating the sample at 70 °C for 10 minutes, electrophoresis was carried out on a 7M urea, 20% polyacrylamide gel for at least 3 hours at 200 volts.

After exposing the gel to X-ray film (Super RX Fujifilm) in the dark for 2-10 minutes (depending on the number of half-lives of the [α - 32 P] ATP isotope that had passed), the appropriate band containing the radiolabeled product was excised from the gel, the gel crushed with a spatula and added to a microfuge tube containing phenol (Fisher). The tube was rotated overnight at 4°C to allow the product to diffuse from the gel slice. The sample was centrifuged at 4 400 xg for 10 minutes at 4°C and the aqueous phase was transferred to a new microfuge tube. Following phenol extraction and ethanol precipitation, the pellet was resuspended in 100 μ L nuclease free water. An aliquot was loaded and electrophoresis was carried out as described above (section 2.5.2) to ensure integrity and purity of product.

2.5.2 Measuring nucleotide addition

Nucleotide addition was measured using a 38 cm by 50 cm 7M urea/12% polyacrylamide gel by the procedure of Leibovitch *et al.* (2013). Prior to loading the samples, electrophoresis was carried out at 2000 volts at room temperature for at least 30 minutes to pre-run the gel. The wells were rinsed with TBE (1X) and the samples (20 μ L) were heated at 70°C for 10 minutes and cooled on ice prior to loading. Electrophoresis was typically for 6-7 hours at 2000 V at room temperature. The gel was placed against a phosphorImager screen (GE Healthcare) for at least 30 minutes (depending on transcript half-lives), the screen was developed and transcripts were detected using the Typhoon™ TRIO Variable Mode Imager (GE Healthcare).

2.5.3 Standard Activity Assays

Procedure modified from Leibovitch *et al.* (2013). In the standard activity assays, 100 mM glycine buffer (pH 9), 10 mM MgCl₂, 1 mM ATP, 0.4 mM CTP, approximately 10 ng of the [α - 32 P] ATP labelled tRNA transcript and 1-50 ng of protein were used. The reactions were initiated with the addition of protein and stopped with 10 μ L of Peattie's (2X) loading dye (Peattie, 1979) after two minutes. Samples were heated to 70°C for 10 minutes, cooled prior to loading onto a 50 cm x 32 cm 7M urea 12% acrylamide gel, and electrophoresed for 6-7 hours at 2000 Volts. The nucleotide addition for each reaction was measured as above (section 2.5.2).

2.5.4 Standard Kinetic Assays

In the kinetic assays, one of the substrate concentrations was varied while the other two concentrations were kept constant at the values indicated in section 2.5.4 (typical baker's yeast tRNA concentration of 100 ng/ μ L when not varied). Each assay tube contained enough reagents for two to three individual assays. At each time point, 10 μ L of the assay mixture was removed and treated as described (section 2.5.4). The ratio of reactant to product (tRNA-NCC/tRNA-NCCA or tRNA-NC/tRNA-NCC) was measured by densitometry (ImageQuant software) and initial rates were determined for varied amounts of tRNA substrate, CTP or ATP. When kinetic parameters were calculated for CTP or ATP the tRNA^{ASP} substrate lacking the terminal CMP residue or AMP residue, respectively were used. Kinetics parameters such as K_m and V_{max} values were calculated using GraFit 7 (Leatherbarrow, 2009). The turnover number (k_{cat}) values were calculated using the equation: $k_{cat} = V_{max}/E_T$, where V_{max} is the rate of substrate conversion to product (expressed as moles per liter per second) and E_T is the total enzyme concentration (in moles per liter) in the reaction tube. The operating protein concentrations for kinetic assays were between 1-200 ng/ μ L depending on activity while the assay times varied between 2 and 30 minutes.

2.5.5 Standard Activity Assay with variable metal ions and to investigate NTP misincorporation

Standard assay conditions (section 2.5.4) were followed, however, the 10 mM MgCl₂ cofactor was replaced by either 10 mM MnCl₂, CaCl₂, or CoCl₂. These assays were repeated in the presence of ATP or CTP or with both, using the tRNA-N transcript (to monitor complete CCA addition or C-addition at position 74) or the NCC-transcript (to monitor A-addition at position 76). The assay time was increased to 30 minutes giving enough time for the reaction to go to completion.

The misincorporation of nucleotide triphosphates was investigated with the N-transcript, NC-transcript or NCC-transcripts in the presence of either 10 mM MgCl₂ or 10 mM CaCl₂. The NTPs (ATP at 1 mM, CTP at 0.4 mM, GTP at 1 mM or UTP at 0.4 mM) were used and tested for each transcript (tRNA-N, tRNA-NC or tRNA-NCC) to monitor the misincorporation when either Mg²⁺ (10 mM) or Ca²⁺ (10 mM) was used as the cofactor.

2.6 Molecular modeling and visualization

A homology modeling server Phyre2 (Protein Homology/analogy Recognition Engine) (Kelly *et al.*, 2015) was used to compare other solved crystal structures of Class II tRNA-NTs to develop a probable structure of yeast tRNA-NT. All of the models were visualized using the molecular visualization software PyMOL (Schrödinger).

The Phyre2 server accepts the protein sequence and generates the best scoring structure as a protein data bank (pdb) file. The pdb file was visualized using PyMOL (Schrödinger).

2.7 Proteolysis Experiments

Several variables including temperature, protease volume and the presence and absence of RNase A treatment before proteolysis were tested to optimize the proteolysis experiments. Lyophilized α -chymotrypsin (SigmaAldrich) provided by Dr. Neema Chirwa was used to prepare a stock concentration of 2 mg/mL in PBS (1X) which was diluted 16 fold before each experiment. When protein samples were RNase A treated (to avoid tRNA interference), the samples were also thoroughly dialyzed in 1X PBS and centrifuged to avoid aggregates. To a volume of 84 μ L of protein (approximately 200 ng/ μ L) in PBS (1X), 6 μ L chymotrypsin (0.125 U/ μ L) was added to initiate proteolysis. At every time point an aliquot (16 μ L) of the reaction mix was transferred to a microfuge tube containing 4 μ L of SDS loading buffer (5X) to stop the reaction. Each sample was boiled for 2-5 minutes and the cleavage pattern was analyzed using SDS-PAGE (as per section 2.3.5).

3.0 RESULTS

3.1 Characterization of growth phenotypes.

As our previous studies (Shan *et al.*, 2008, Goring *et al.*, 2013) have shown that changing the glutamate residue at position 189 of the yeast tRNA nucleotidyltransferase to lysine or phenylalanine (but not glutamine) resulted in a temperature-sensitive (ts) phenotype which could be suppressed by converting arginine at position 64 to tryptophan (replicated in Fig. 3-1), we wanted to determine whether other alterations at or around position 189 could generate the ts phenotype. Here we show that strains carrying the E189A, D190A and D190F (but not V188A) substitutions show the ts phenotype (D190F unable to grow at either temperatures) that can be suppressed by the R64W change (Fig. 3-1).

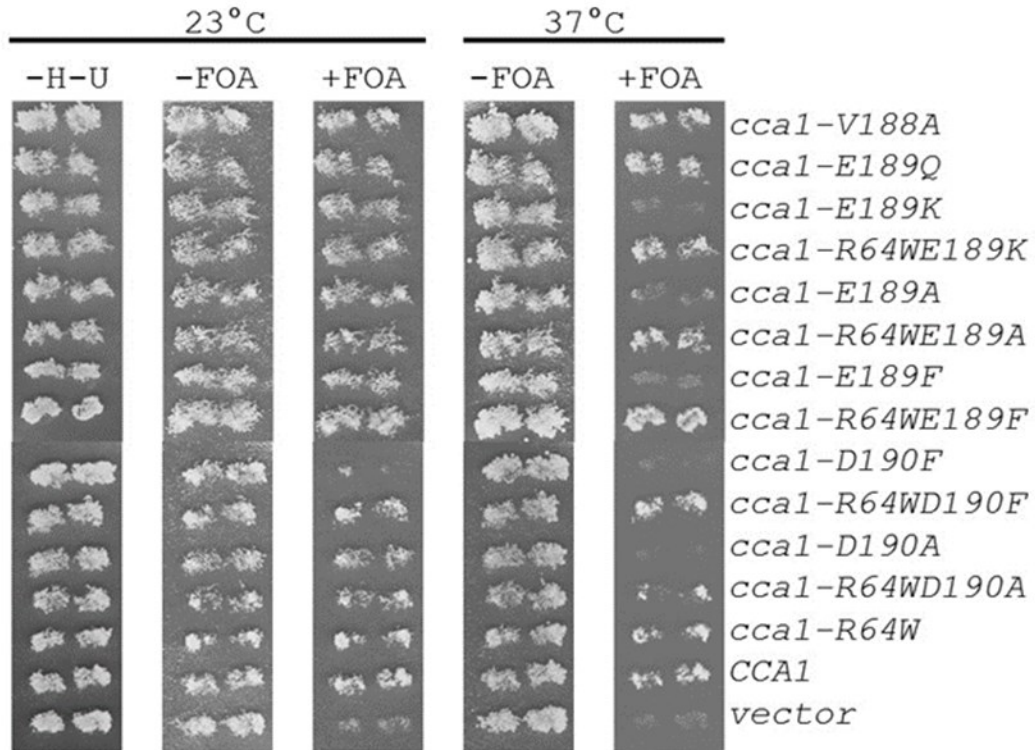


Figure 3-1: Growth of yeast expressing native and variant tRNA nucleotidyltransferases. Yeast strain E189F was transformed with plasmids coding for the tRNA nucleotidyltransferase proteins indicated and two independent transformants were first grown on SC medium lacking uracil and histidine (-H-U) and then replica-plated to FOA medium containing (+FOA) or lacking (-FOA) 5-fluoro-orotic acid and incubated at 23°C or 37°C to assess temperature sensitivity. These data were provided by Dr. Pamela Hanic-Joyce.

3.2 Protein Purification

To explore how these new amino acid substitutions affected the tRNA nucleotidyltransferase enzyme we set out to purify the proteins for biophysical and biochemical characterization. After heterologous expression in *E. coli*, glutathione sulfotransferase-tagged tRNA-NT was collected from cell lysates. Appropriate fractions were pooled and digested with thrombin (GE Healthcare). After thrombin cleavage, the samples were passed through the GST column again to remove any undigested fusion protein and free GST. Three passes through the column were sufficient to remove almost all of the GST-containing proteins. Example SDS-PAGE gels are shown in Fig. 3-2; and Fig. 3-3 shows the level of purity of all of the proteins generated and analyzed in this study.

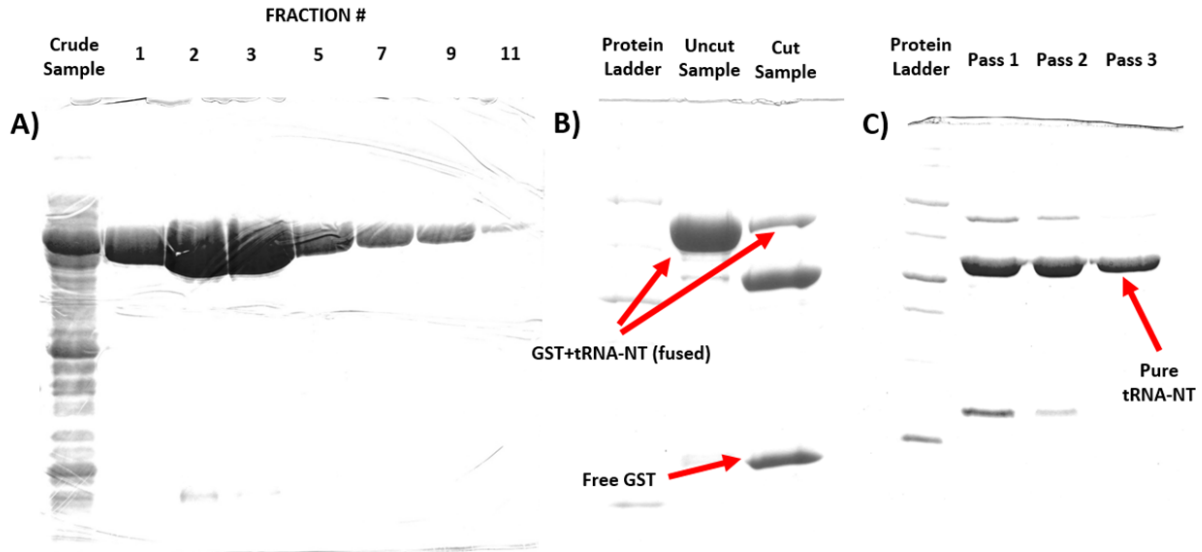


Figure 3-2: Purification of native tRNA nucleotidyltransferase. A) Fractions collected after addition of 15 mM glutathione to a GST-column. B) Cleavage of GST-tagged tRNA-NT by thrombin. C) Removal of GST-tagged tRNA-NT and GST from tRNA-NT by additional passes through the GST column

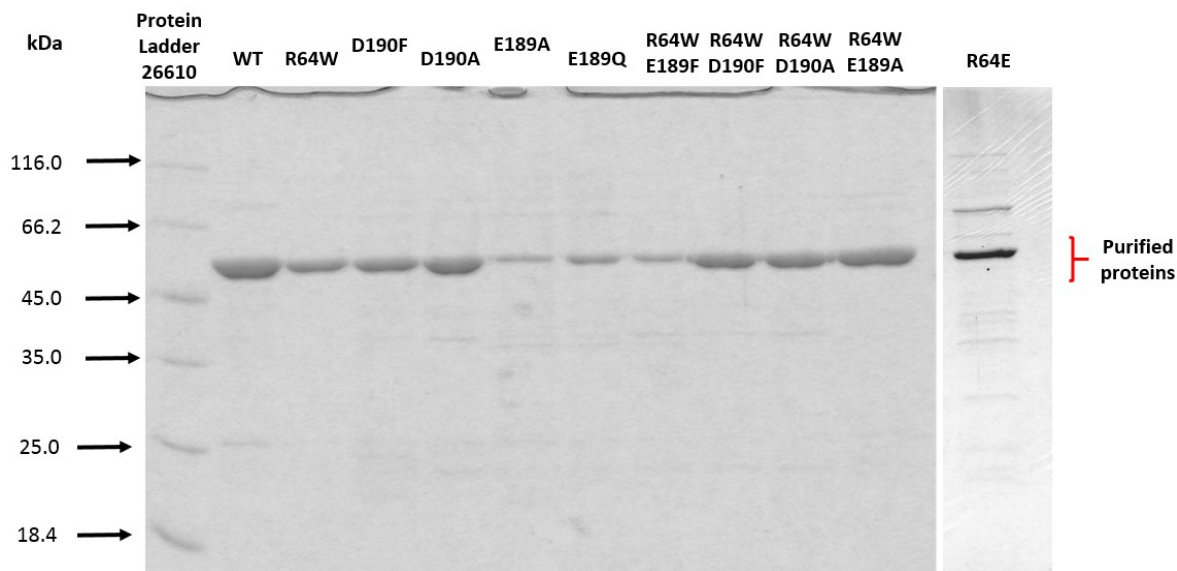


Figure 3-3: Level of purity of native and variant tRNA nucleotidyltransferases used in this study. All of the samples were purified as GST-tagged fusion proteins and the GST portion removed by cleavage with thrombin. The proteins were separated by SDS-PAGE and stained with Coomassie blue. Ladder, PageRuler™ unstained Broad Range Protein Ladder 26610 (Thermo Scientific). The proteins loaded in each lane represent 16 μ L from every 12 mL of purified protein. The protein concentrations determined using Bradford Assay (BioRad) are included in the Appendix (Fig. 7-1).

3.3 Biophysical Characterization of native and variant tRNA-NT enzymes

3.3.1 Effect of amino acid substitutions at positions 64, 189 and 190 on circular dichroism spectra

Initially, we were interested in determining whether these amino acid substitutions resulted in any secondary structure changes, which could be measured as changes in CD signal. All of the proteins were RNase A treated and extensively dialyzed overnight in PBS to avoid any influence on the spectra from tRNA molecules associated with the proteins. All of the spectra (Fig. 3-4) show the double-trough feature with minima at 208 nm and 222 nm characteristic of proteins showing primarily α -helical character (Berg *et al.*, 2010). Only the E189A spectrum (with a greater minimum at 222 nm than at 208 nm) shows any difference from the native spectrum. All of the other spectra overlay with only small differences that may simply reflect discrepancies in estimating the concentration of each protein.

Secondary structure using CD

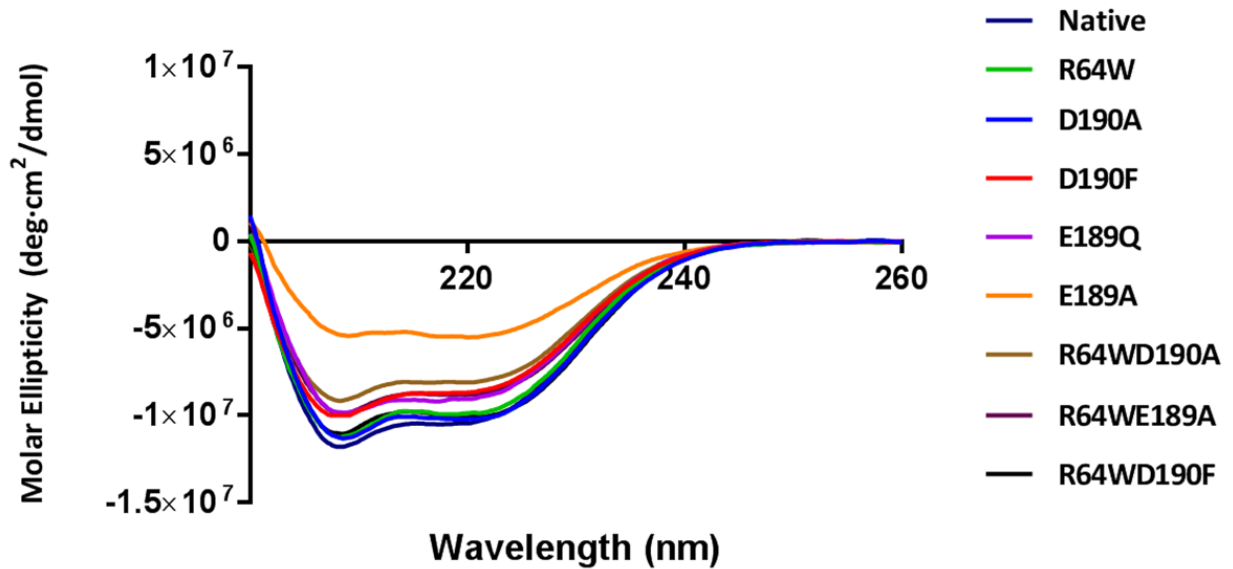


Figure 3-4: Overlay of peptide backbone scans of native and variant tRNA nucleotidyltransferases. Each enzyme is color coded as shown in the legend (on the right). The spectra were recorded between 200-260 nm at 20°C. The protein concentrations were normalized to convert circular dichroism signals to molar ellipticity.

3.3.2 Effect of amino acid substitutions at positions 64, 189 and 190 on thermal stability

As we previously had shown that changing the glutamate at position 189 to lysine or phenylalanine reduced the melting temperature (T_m) of the enzyme, we wanted to see what effect the new mutations would have on the T_m . To explore this, the change in α -helical content as a function of increasing temperature was monitored using circular dichroism (CD) spectroscopy. Changes in CD signal at 222 nm were monitored as the temperature was increased as at this wavelength the minimum is defined solely by α -helices. These values were used to calculate the fraction of unfolded protein using the formula as explained in section 2.4.1.2. As illustrated below in the thermal denaturation profiles (Fig. 3-5), the melting temperature (T_m) that reflects the temperature at which 50% of the protein has unfolded was calculated (Table 3-1). Unlike the decrease in T_m of more than 6°C that we had seen previously for the E189K and E189F variants (Shan *et al.*, 2008), we saw a maximum decrease in T_m of only 2.5°C (R64WE189A) for the proteins studied here and in fact the E189A variant actually showed an increase in T_m of about 5°C. The T_m values calculated here for the native enzyme and the R64W and E189Q variants are in good agreement with our previous results (Shan *et al.*, 2008, Goring *et al.*, 2013) highlighting the reproducibility of this experiment.

Although the T_m values calculated for the D190F and R64WD190F variants are within experimental error of that of the native enzyme (Table 3-1), they show slightly altered thermal denaturation profiles (Fig. 3-5) suggesting differences in their unfolding patterns after reaching their respective T_m s. After the sample temperature had been increased from 20°C to 80°C during the course of the thermal denaturation experiment, it was returned to 20°C and an additional CD spectrum between 200-260 nm was collected. These spectra showed that the characteristic α -helical signals were lost, suggesting complete denaturation (data not shown). Moreover, after each thermal denaturation experiment white precipitates accumulated indicative of denatured proteins coming out of solution.

Thermal Denaturation Profiles

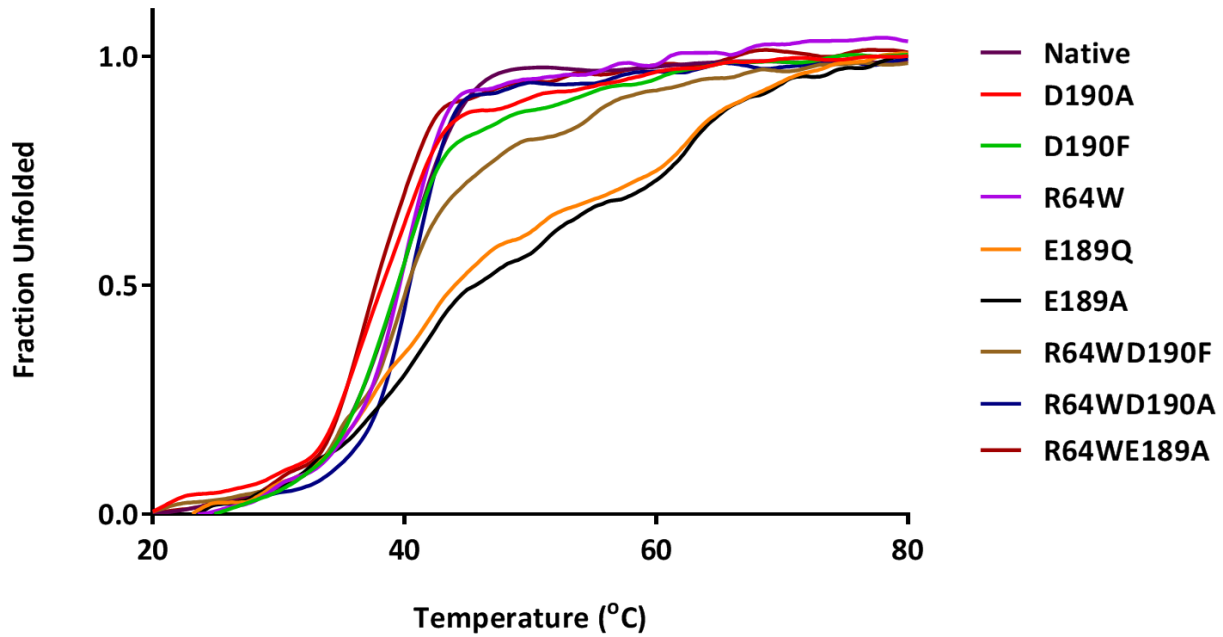


Figure 3-5: Overlay of thermal denaturation profiles of native and variant tRNA nucleotidyltransferases defined using circular dichroism spectroscopy. Each denaturation profile is color coded according to the legend (on the right).

Protein	T_m (°C)
Native	40.3 ± 0.6
D190A	38.3 ± 0.3
D190F	39.5 ± 0.4
R64W	39.6 ± 0.3
E189Q	43.8 ± 0.6
E189A	45.2 ± 0.5
R64WD190F	40.3 ± 0.3
R64WD190A	40.4 ± 0.4
R64WE189A	37.8 ± 0.3

Table 3-1: T_m values (with standard deviation) calculated from the thermal denaturation profiles of native and variant tRNA nucleotidyltransferases.

3.4 Effect of amino acid substitutions at positions 64, 189 and 190 on intrinsic fluorescence

As the E189F and E189K changes resulted in a shift in wavelength of maximum fluorescence signal of 8-9 nm after excitation at 280 nm (Shan *et al.*, 2008), we wanted to see if a similar change would be apparent in the new variants. After excitation of tryptophan and tyrosine residues at 280 nm and exclusively tryptophan residues at 295 nm, the fluorescence emission spectrum for each enzyme was measured at 20°C between 310-400 nm (Fig. 3-6). An overlay of the emission spectra shows that while most proteins show emission spectra with intensities within 30% of that of the native enzyme, the E189A variant has an emission profile dramatically different from the native enzyme with an intensity more than 100% less than the native enzyme (Fig. 3-6). This is consistent with the CD data (Fig. 3-5), where the E189A variant gave a reduced signal. It is interesting that the total number of tryptophan residues in the native enzyme is five, and that the addition of a sixth tryptophan in the R64W variants did not result in greater fluorescence intensity as compared to the native enzyme (Fig. 3-7).

Within experimental error, there was no difference in the wavelength of maximum fluorescence intensity when only the tryptophan residues were excited at 295 nm (Table 3-2). However, excitation of both tryptophan and tyrosine residues at 280 nm resulted in an approximately 9 nm red shift for the E189K and E189F variants as had been seen previously (Shan *et al.*, 2008).

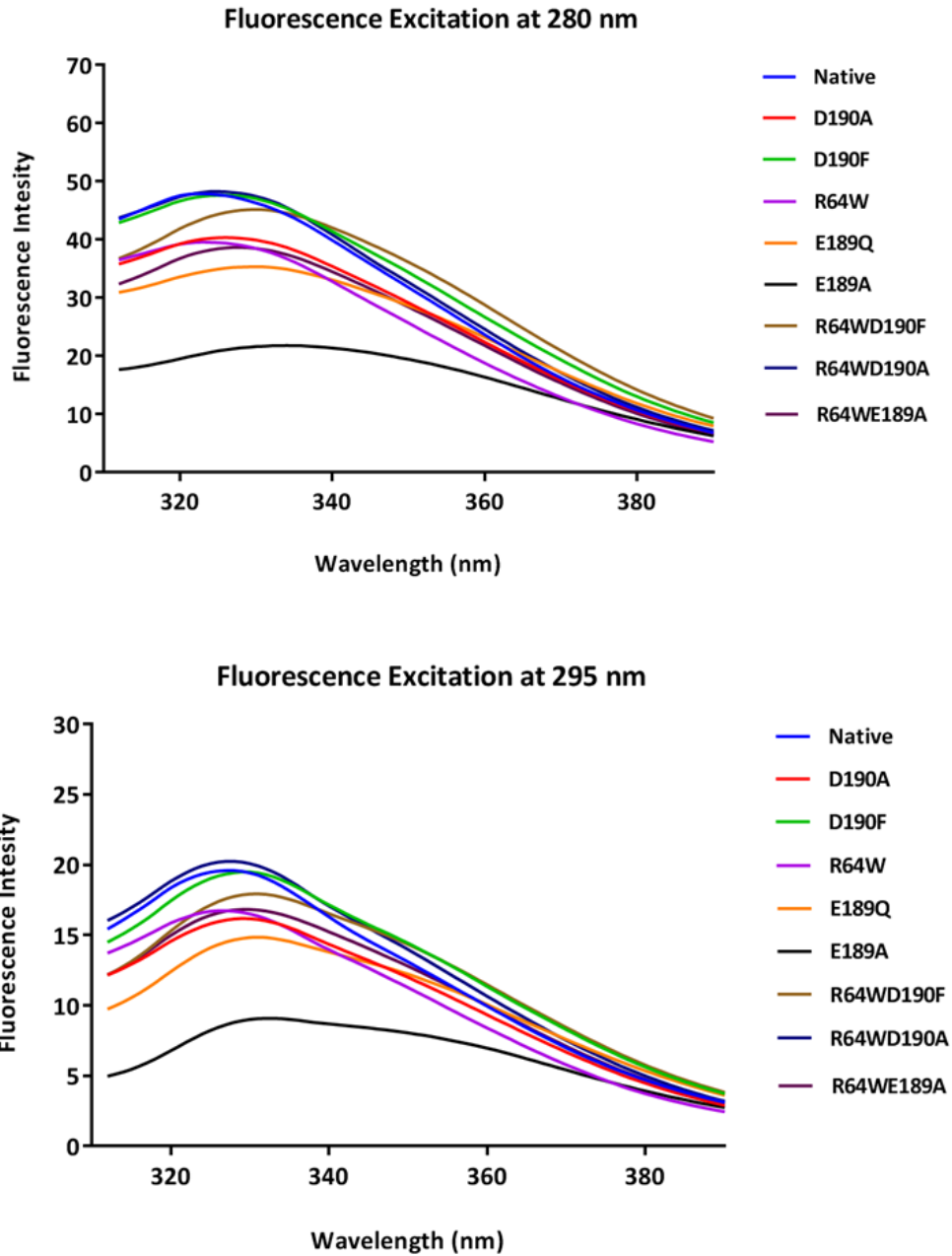


Figure 3-6: Overlay of fluorescence emission spectra for native and variant tRNA nucleotidyltransferases excited at 280 nm or 295 nm. The fluorescence emission for each enzyme was measured at 20°C between 310-400 nm. All of the variants are color coded according to the legend (on the right). At both excitation wavelengths, the native and variant proteins exhibited similar spectra except for E189A, which shows lower fluorescence intensity.

Fluorescence Maxima λ (nm)		
Protein	Excited at 280 nm	Excitation at 295 nm
Native	322 \pm 2	328 \pm 1
D190A	328 \pm 1	330 \pm 1
D190F	327 \pm 1	329 \pm 1
R64W	329 \pm 1	328 \pm 2
E189Q	331 \pm 2	329 \pm 1
E189A	329 \pm 1	330 \pm 1
RWDF	329 \pm 2	330 \pm 1
RWDA	328 \pm 1	329 \pm 1
RWEA	329 \pm 1	329 \pm 1

Table 3-2: Wavelength (\pm standard deviation) of fluorescence emission maximum of native or variant tRNA nucleotidyltransferases.

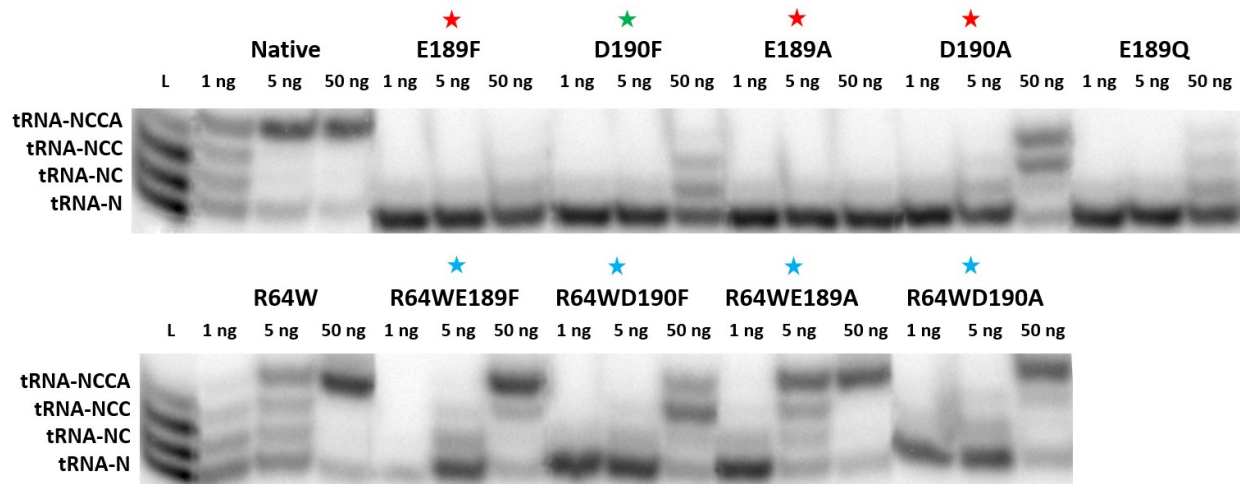
3.5 Effect of amino acid substitutions at positions 64, 189 and 190 on enzyme activity

As we previously had shown that changing position E189 to lysine or phenylalanine resulted in a greater than 20-fold decrease in enzyme activity (Shan *et al.*, 2008) and specifically a reduction in turnover number (Goring *et al.*, 2013) we wanted to see how additional changes in this region of the protein would affect activity. Initially, a qualitative enzyme assay was carried out at 20°C (assay time: 2 mins) under standard conditions of substrate concentrations (see section 2.5.4) with increasing amounts of enzyme to determine the relative activity of each variant. As expected, the native enzyme was the most efficient with approximately 50% complete CCA addition even at the lowest protein amount (1 ng) tested (Fig. 3-7). Increasing the amount of native enzyme by only five fold to 5 ng was sufficient to convert all of the substrate to product. As had been shown previously (Goring *et al.*, 2013), the R64W variant has reduced activity but still was able to convert 10% of the substrate to product while accumulating good levels of C and CC intermediates (26% and 20%, respectively) at 1 ng of enzyme. All of the other single variants showed undetectable levels of CCA addition at 1 ng protein levels and, in fact, some (E189F and E189A) showed no product formation even at 50 ng enzyme (Fig. 3-7).

These data are consistent with what we had seen previously with the E189F variant and correlate well with the fact that these variants were responsible for exhibiting the *ts* phenotype. Although the D190A variant showed some activity with 43% complete CCA addition at 50 ng of protein, it still showed a *ts* phenotype *in vivo*. The D190F variant which showed limited or no growth at both the permissive and restrictive temperatures (Fig. 3-1) actually seemed to have retained more activity (2.0% complete CCA-addition, and 19% CC-addition at 5 ng and 50 ng of protein, respectively *in vitro*) than the E189F and E189A variants which grew well at the permissive temperature.

As we had previously shown that a second site substitution increased the activity to the E189F variant (Goring *et al.*, 2013), we wanted to determine if a similar increase in activity could be seen for the new variants generated here. This was indeed the case as all four variants (E189F, E189A, D190F and D190A) showed increased activity when combined with the R64W change (Fig. 3-7). The E189A variant, for example, which alone had shown zero activity even at 50 ng of protein

now when combined with the R64W substitution, had 83% complete CCA addition. A similar increase was observed with R64WE189F (78% complete CCA addition) and to some extent R64WD190F (23% complete CCA addition). Interestingly, R64WD190A showed the least “restoration” of activity with only small differences in activity at 1 ng and 5 ng of protein and an increase from 43% to 63% complete CCA addition at 50 ng of protein.



- ★ → ts phenotype (no growth of mutants at 37°C)
- ★ → lethal (no growth of mutants at either 23°C or 37°C)
- ★ → ts suppressed (growth of cells at both 23°C and 37°C)

Figure 3-7: Qualitative enzyme activity assays on native and variant tRNA nucleotidyltransferases. On the left indicates the possible products tRNA-NC, tRNA-NCC and tRNA-CCA, or unreacted tRNA-N transcripts. Enzyme names and amounts are indicated above each lane. A red star indicates a temperature-sensitive variant and a blue star denotes the variants in which the temperature-sensitive phenotype was suppressed; the green star denotes low or no growth at both the permissive and restrictive temperatures.

Protein		Native			R64W		
	1 ng	5 ng	50 ng	1 ng	5 ng	50 ng	
tRNA-NCCA	48	80	92	10	37	84	
tRNA-NCC	16			20	12		
tRNA-NC	16			26	12		
tRNA-N	20	20	8	44	39	16	

Protein		E189F			R64WE189F		
	1 ng	5 ng	50 ng	1 ng	5 ng	50 ng	
tRNA-NCCA						78	
tRNA-NCC					8	6	
tRNA-NC			6		12		
tRNA-N	>99	>99	94	>99	80	16	

Protein		D190F			R64WD190F		
	1 ng	5 ng	50 ng	1 ng	5 ng	50 ng	
tRNA-NCCA						23	
tRNA-NCC			19			42	
tRNA-NC			25				
tRNA-N	>99	>99	56	>99	>99	35	

Protein		E189A			R64WE189A		
	1 ng	5 ng	50 ng	1 ng	5 ng	50 ng	
tRNA-NCCA					54	83	
tRNA-NCC					11		
tRNA-NC				4	5		
tRNA-N	>99	>99	>99	96	30	17	

Protein		D190A			R64WD190A		
	1 ng	5 ng	50 ng	1 ng	5 ng	50 ng	
tRNA-NCCA			43			63	
tRNA-NCC		5	34		5	3	
tRNA-NC		10	3		9		
tRNA-N	>99	85	20	>99	86	34	

Protein		E189Q		
	1 ng	5 ng	50 ng	
tRNA-NCCA			8	
tRNA-NCC			8	
tRNA-NC			9	
tRNA-N	>99	>99	76	

Table 3-3: Densitometry data from crude assays of tRNA nucleotidyltransferases. The numbers indicates percentage (%) products (either tRNA-NCCA, tRNA-NCC, tRNA-NC) or unreacted tRNA-N transcript at protein levels of 1 ng, 5 ng and 50 ng. The products which were undetectable are in red and greater than 99% (>99) tRNA-N denotes no activity.

Since these results indicated that all of the variants had retained at least some level of activity, kinetic assays were carried out to obtain more quantitative values. The apparent kinetic parameters for the native and variant enzymes derived from altering the tRNA (Table 3-4), CTP (Table 3-5) or ATP (Table 3-6) concentrations are shown here.

In all cases but one, the turnover number for the native enzyme (regardless of which substrate concentration was varied) was the highest. The one exception was the R64WE189A variant when ATP concentration was varied where the turnover number was about 10% higher than that of the native enzyme (Table 3-6). This may suggest something about variants carrying the E189A substitution which also showed unusual results with the biophysical assays (Fig. 3-4 to 3-6). Excluding the R64WE189A result in the presence of ATP, the R64W variant showed the turnover number closest to that of the native enzyme regardless of which substrate concentration was varied. Moreover, the E189A variant always showed the greatest decrease in k_{cat} (from 100 to 675 fold less than the native enzyme). This dramatic reduction in activity was seen in the qualitative assays (Fig. 3-7) where no product was seen at any enzyme concentration tested. Consistent with what had been seen previously in the yeast (Shan *et al.*, 2008, Goring *et al.*, 2013) and human (Ernst *et al.*, 2015) enzymes, changing the acidic amino acids at the positions corresponding to amino acids 189 or 190 in the yeast enzyme to phenylalanine or alanine resulted in a decrease in activity ranging from 6-fold in the case of the D190A (Table 3-5) substitution to a more than 600-fold decrease in activity for the E189A substitution (Table 3-6).

Of particular interest is the E189Q variant which we previously had shown to retain approximately 40% activity as compared to the native enzyme and which did not show the ts phenotype (Shan *et al.*, 2008). Here this variant showed biophysical characteristics similar to those of the native enzyme (Figs. 3-4, 3-5, 3-6) but had a 20-80 fold reduction in k_{cat} (Table 3-6) in good agreement with the qualitative enzyme assay (Fig. 3-7). Also as seen previously (Goring *et al.*, 2013), the R64W substitution had only a small effect on enzyme activity, here reducing k_{cat} by less than 30% and in combination with any of the other 189 or 190 substitutions restoring activity typically by at least 10 fold. The exception to this is the R64WD190A variant that showed

only a 4-fold or less increase in k_{cat} in the double variant. Again, these data are in good agreement with what was seen in the qualitative results (Fig. 3-7) where there appeared to be only a small increase in product formation in the R64WD190A variant as compared to the D190A variant.

When looking at the K_m values, there are no defined trends when comparing the three different substrates. In each case the native enzyme shows an intermediate K_m value with some variants having lower values (maximum 7-fold lower for CTP) and others having higher values (maximum 4-fold higher for CTP) with most within 3-fold of the native enzyme. The overall variability between K_m values among all variants is approximately 7 fold for tRNA (Table 3-4), eight fold for ATP (Table 3-6) and 29 fold for CTP (Table 3-5). In none of the cases, did the same variant show the highest K_m value for all three substrates, but in each case a double variant shows the lowest K_m for each specific substrate; ATP (R64WD190A), CTP (R64WE189A), tRNA (R64WD190F). The apparent K_m values calculated here for the native enzyme (830 μ M for CTP and 72 μ M for ATP) are in good agreement with the values (560 μ M and 180 μ M, respectively) determined previously (Chen *et al.*, 1990) for the yeast enzyme.

Given the relatively small changes seen in K_m for most of the variants for ATP, CTP and tRNA in comparing the variants to the native enzyme (typically less than 7 fold) and the larger changes generally seen in k_{cat} (up to 100 fold), the relative differences among the specificity constants in all cases tended to follow the trend defined by the k_{cat} values. In most cases the specificity constants were within one order of magnitude of that of the native enzyme and surprisingly in the case of the R64WE189A double variant, the specificity constants when ATP (Table 3.6) or CTP (Table 3.5) concentrations were varied were even higher than that of the native enzyme.

Enzyme	K_m (μM)	k_{cat} (s^{-1})	k_{cat}/K_m ($\mu\text{M}^{-1}.\text{s}^{-1}$)
Native	1.4 ± 0.49	1.1	0.83
R64W	2.2 ± 0.62	0.9	0.42
E189F	1.8 ± 0.56	0.017	0.010
D190F	0.70 ± 0.090	0.0040	0.0060
D190A	1.9 ± 0.39	0.17	0.089
E189A	3.9 ± 0.62	0.0030	0.0010
E189Q	0.65 ± 0.15	0.014	0.022
R64WE189F	1.7 ± 0.50	0.099	0.057
R64WD190F	0.58 ± 0.13	0.079	0.14
R64WD190A	1.5 ± 0.66	0.62	0.40
R64WE189A	1.3 ± 0.26	0.74	0.59

Table 3-4: Summary of apparent kinetic parameters defined for native and variant tRNA nucleotidyltransferases when the tRNA concentration was varied. The R64W, E189F and R64WD189F kinetic data were provided by Dr. Matthew Leibovitch.

Enzyme	K_m (μM)	k_{cat} (s^{-1})	k_{cat}/K_m ($\mu\text{M}^{-1}.\text{s}^{-1}$)
Native	72 \pm 17	2.7	0.037
R64W	22 \pm 4.9	2.0	0.088
E189F	180 \pm 29	0.030	0.00017
D190F	290 \pm 62	0.031	0.00011
D190A	110 \pm 20	0.44	0.0040
E189A	170 \pm 40	0.0040	0.000020
E189Q	96 \pm 21	0.037	0.00039
R64WE189F	42 \pm 7.8	0.31	0.0075
R64WD190F	200 \pm 39	0.85	0.0043
R64WD190A	180 \pm 36	1.0	0.0057
R64WE189A	10 \pm 2.1	1.7	0.16

Table 3-5: Summary of apparent kinetic parameters defined for native and variant tRNA nucleotidyltransferases when the CTP concentration was varied. The R64W, E189F and R64WD189F kinetic data were provided by Dr. Matthew Leibovitch.

Enzyme	K_m (μM)	k_{cat} (s^{-1})	k_{cat}/K_m ($\mu\text{M}^{-1}.\text{s}^{-1}$)
Native	830 \pm 160	1.2	0.0015
R64W	890 \pm 200	1.0	0.0012
E189F	890 \pm 150	0.019	0.000020
D190F	650 \pm 130	0.011	0.000020
D190A	880 \pm 370	0.17	0.00019
E189A	810 \pm 130	0.0090	0.000010
E189Q	780 \pm 230	0.057	0.000070
R64WE189F	1400 \pm 460	0.16	0.00011
R64WD190F	2100 \pm 650	0.90	0.00043
R64WD190A	260 \pm 29	0.19	0.00074
R64WE189A	410 \pm 58	1.32	0.0032

Table 3-6: Summary of apparent kinetic parameters defined for native and variant tRNA nucleotidyltransferases when the ATP concentration was varied. The R64W, E189F and R64WD189F kinetic data were provided by Dr. Matthew Leibovitch.

3.6 Role of metal ions in defining recognition of ATP or CTP in native and R64W enzymes

Since motif A contains two aspartic acid residues that coordinate the metal ions required for catalysis as well as conserved glycine and arginine residues that bind the triphosphate of the incoming ATP or CTP (Li *et al.*, 2002) and as R64 is found in motif A, we explored the effect of substituting different divalent cations (Mg^{2+} , Mn^{2+} , Co^{2+} or Ca^{2+}) on enzyme activity. These assays were carried out under standard conditions (Section 2.5.6) except that in some cases Mn^{2+} , Co^{2+} or Ca^{2+} replaced the Mg^{2+} cofactor. For each metal ion, either the tRNA-N transcript (addition of 74th position or complete addition monitored), or the tRNA-NCC transcript (addition of 76th position monitored) was tested. A third reaction (control) involved the tRNA-N transcript with both CTP and ATP provided to see complete CCA-addition. This experiment allowed us to compare both the efficiency and specificity of the native and R64W variant enzymes in the presence of these different divalent cations (Fig. 3-8).

Even though both the native and R64W variant enzymes were able to use either cobalt or manganese ions as cofactor for complete CCA addition (albeit not as efficiently as with magnesium), calcium shows little to no complete CCA addition (ATP + CTP lane). The more interesting observations are evident in terms of misincorporation of nucleotides (involving ATP or CTP alone). Under standard assay conditions (with Mg^{2+} as cofactor) the native enzyme misincorporates AMP (in place of the first CMP) relatively well (75%) and a second AMP (in place of the second CMP) to some degree (7%) into the tRNA-N transcript. Similarly, a high amount of CMP misincorporation (83%) was observed in place of AMP in the third position using the tRNA-NCC transcript. This is in good agreement with what we have seen previously in our qualitative assays (Goring *et al.*, 2013).

Similarly, for the R64W variant two AMP residues are more efficiently misincorporated into the tRNA-N transcript (55% tRNA-NAA) than they are when the native enzyme is used. Moreover, CMP misincorporation was comparable to the native enzyme (74% tRNA-NCCC) using the tRNA-NCC transcript. Upon using cobalt ions, we see an even greater misincorporation of two AMP residues into the tRNA-N template by the R64W enzyme (68% tRNA-NAA) compared to the native

enzyme (31% tRNA-NAA). However, the misincorporation of CMP into the tRNA-CC template are comparable (89% and 85% tRNA-NCCC formed for native and R64W enzymes, respectively).

Strikingly, when manganese is used as the cofactor, both the native and R64W variant enzymes show a limited degree of misincorporation with either template. The native enzymes and R64W enzymes produced 3% and 5% tRNA-NAA product, respectively, while no misincorporation of CMP to produce tRNA-NCCC (using tRNA-NCC template) is observed. Finally, the reduced level of activity seen when calcium is used as the divalent cation did not allow any measurable level of misincorporation to be recorded with the R64W variant protein or the native enzyme (Table 3-7).

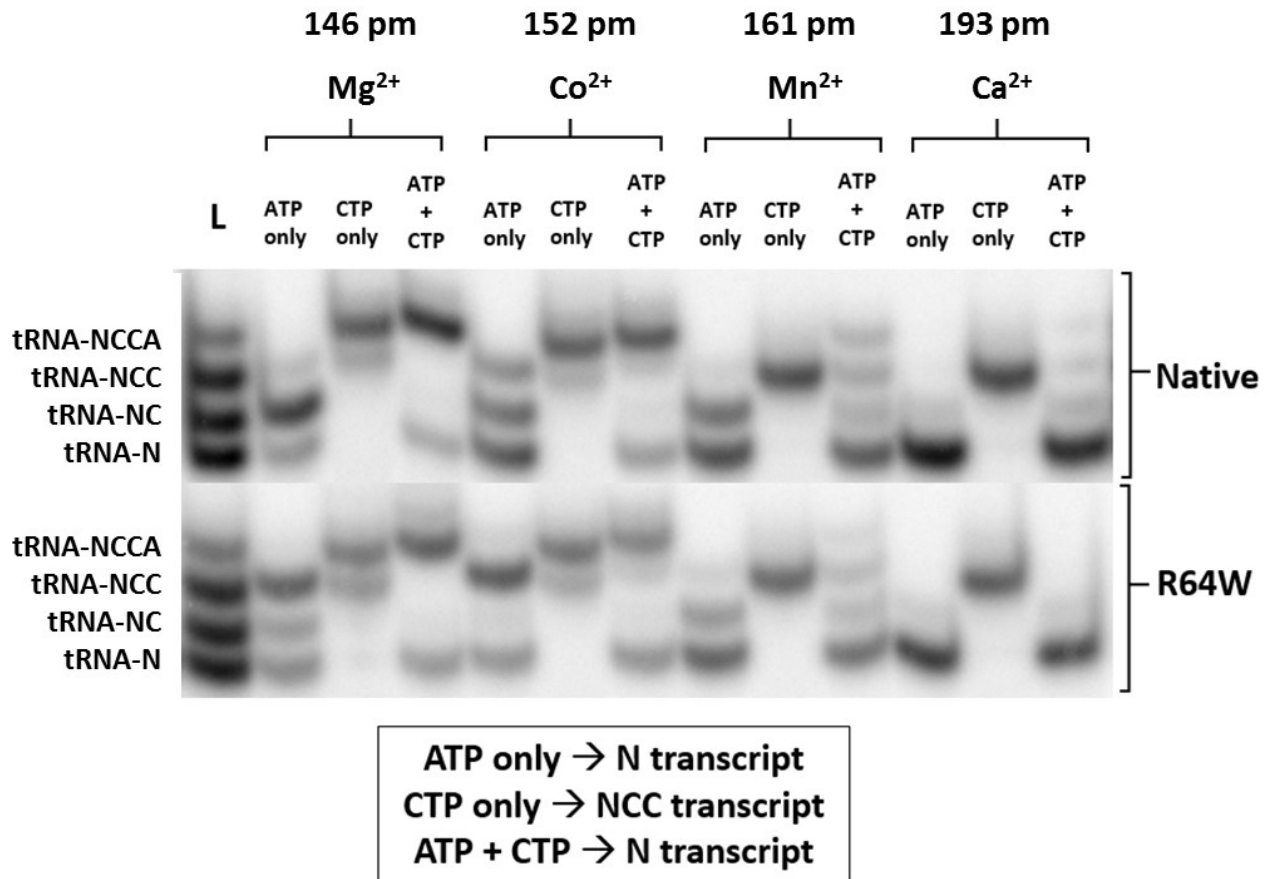


Figure 3-8: Incorporation of AMP and/or CMP in the presence of different divalent cations. The assays were done in our standard 10 μ L reaction volume with 5 ng of protein and a reaction time of 30 minutes. The left lane shows the RNA ladder (tRNA-N, tRNA-NC, tRNA-NCC, and tRNA-NCCA). The metal ions used are labelled above the gel with their ionic radii. The tRNA-N transcript was used for reactions involving either only ATP (AMP misincorporation monitored) or both ATP and CTP (CA-addition monitored) whereas, the tRNA-NCC transcript was used with CTP (CMP misincorporation monitored).

WT	Mg ²⁺			Co ²⁺			Mn ²⁺			Ca ²⁺		
	A	C	A+C									
tRNA-NCCA		83	82		89	77			18			3
tRNA-NCC	7	17		31	11	2	3	>99	17		>99	7
tRNA-NC	75	N/A		28	N/A		42	N/A	6	4	N/A	6
tRNA-N	18	N/A	18	41	N/A	21	55	N/A	59	96	N/A	84
R64W	Mg ²⁺			Co ²⁺			Mn ²⁺			Ca ²⁺		
	A	C	A+C									
tRNA-NCCA		74	72		85	47			5			
tRNA-NCC	55	26		68	15		5	>99	13		>99	
tRNA-NC	12	N/A			N/A		36	N/A	7	3	N/A	2
tRNA-N	33	N/A	28	32	N/A	53	59	N/A	76	97	N/A	98

Table 3-7: Densitometry data from crude assays of tRNA nucleotidyltransferases using variable metal ions as cofactor. The numbers indicate percentage (%) products (either tRNA-NCCA, tRNA-NCC, tRNA-NC or misincorporated products) or unreacted tRNA-N transcript at protein level 5 ng. The products which were undetectable are in red, and greater than 99% (>99) denotes “no activity” or all unreacted tRNA-N transcript; and the letters A and C denote ATP and/or CTP added to that particular assay mix. Samples labeled N/A were not tested.

3.7 Nucleotide triphosphate substrate specificity with Mg²⁺ or Ca²⁺ ions in native and R64W enzymes

Noting the level of misincorporation of AMP and CMP for the native and R64W variant enzymes when either magnesium or calcium was used as the cofactor we decided to determine if misincorporation could be extended to UTP or GTP. The experiment was carried out under standard conditions, except that when calcium was used as cofactor the amount of protein was increased 20-fold (100 ng) to account for the reduced activity seen in the presence of calcium. In the assays each template (tRNA-N, tRNA-NC or tRNA-NCC) was tested with a single nucleotide triphosphate (ATP, CTP, GTP or UTP) to monitor addition to the first, second or third position.

In the control experiment with magnesium as cofactor, misincorporation of all four NTPs was evident (Fig. 3-9). As we had seen previously (Fig. 3-8), both the native enzyme and the R64W variant incorporated one to two AMP residues or three CMP residues into the tRNA-N template (Fig. 3-9). While neither enzyme was able to incorporate much GMP into this template, both were able to incorporate at least one UMP. With the tRNA-NC template both enzymes were able to add two AMP, two CMP residues, or one UMP residue but essentially no GMP residues. With the tRNA-NCC template, both enzymes could efficiently add AMP, CMP, and UMP but not GMP. When the experiment was repeated using calcium as the cofactor there was no obvious misincorporation of any NTP even after increasing the amount of protein 20 fold (Fig. 3-9).

3.8 Fluorescence quenching of tryptophan fluorescence in the native and R64W proteins by ATP or CTP to determine K_d

Fluorescence quenching experiments with either ATP or CTP were performed to determine dissociation constants (K_d) for ATP and CTP. Upon addition of increasing quantities of ATP or CTP to the purified protein sample, the overall fluorescence intensity diminished. These decreases in fluorescence intensity (Fig. 3-10) were corrected for the inner-filter effect using the formula in section 2.4.3 to calculate the K_d .

As shown in Table 3-6, the dissociation constants for ATP and CTP are approximately equal and differ by approximately two fold between the native and R64W enzymes. Although in both cases the K_d values were lower for the R64W variant than for the native enzyme, the difference is small. However, these data are consistent with the kinetics data (section 3.6), which show a maximum 3-fold difference in K_m for ATP or CTP between the native and R64W proteins.

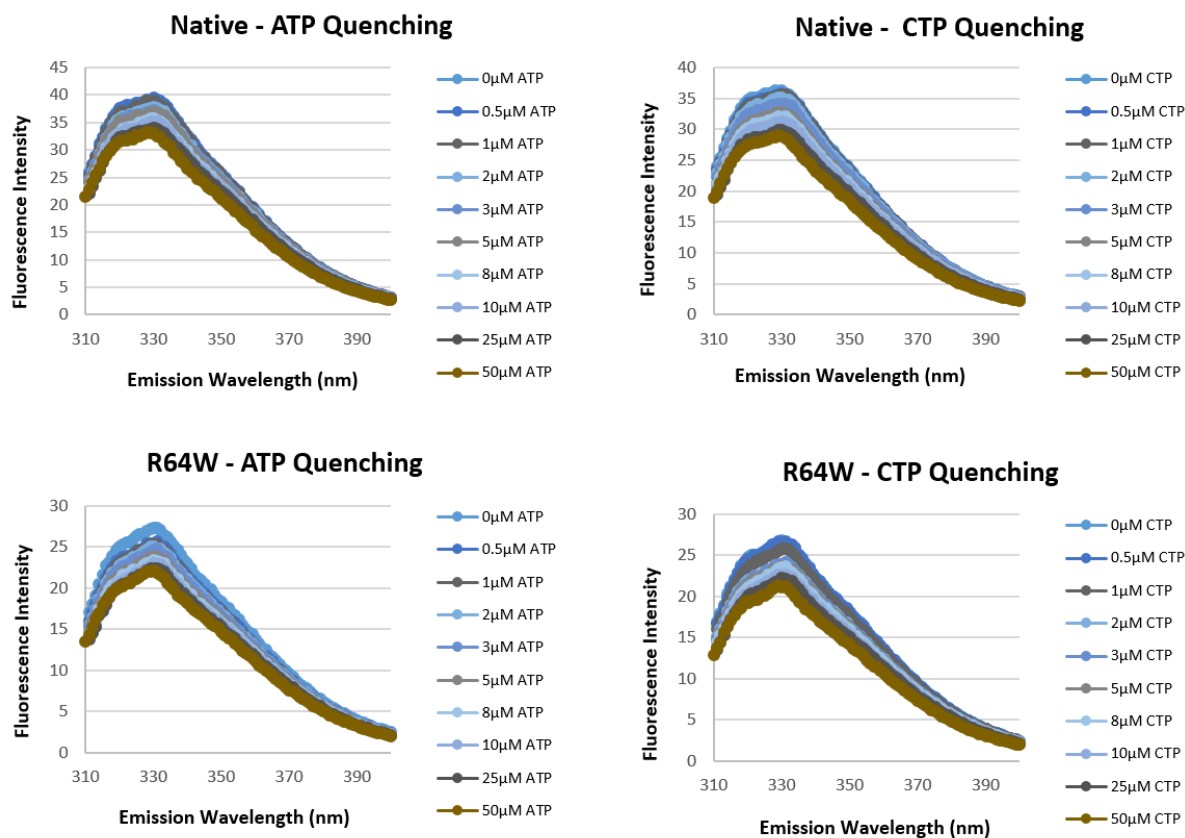


Figure 3-10: Fluorescence Quenching with ATP or CTP of native and R64W enzymes.

	ATP	CTP
Enzyme	K_d (μM)	K_d (μM)
Native	6.7 ± 1.2	6.2 ± 0.61
R64W	2.6 ± 0.51	2.3 ± 0.38

Table 3-8: Dissociation constants for ATP or CTP using the native or R64W enzymes. The drop in fluorescence intensity from the quenching experiments was recorded and after correcting for the inner-filter effect, the dissociation constant of native and R64W enzymes were acquired using GraFit 7.

3.9 Proteolysis

3.9.1 SDS-PAGE Results of Proteolysis with Chymotrypsin

All of the biochemical and biophysical experiments (*e.g.*, CD and fluorescence spectroscopy, thermal denaturation, metal ion substitution, fluorescence quenching) were designed to investigate structural or functional changes in the enzyme resulting from amino acid substitutions at positions 64, 189 and 190. While amino acid substitutions at positions 189 and 190 reduced enzyme activity, second site substitutions at position 64 typically increased the activity of these variants (Table 3-4, 3-5 and 3-6) and suppressed the ts phenotype (Fig. 3-1). While neither CD (Fig. 3-4) nor fluorescence (Fig. 3-6) spectroscopy suggested that the R64W change altered enzyme structure, we wanted to try another approach to check this. Here we used proteolysis assuming that if the conformation of the enzyme had changed even slightly a new proteolytic cleavage site might be exposed or masked. We chose to test this with bovine α -chymotrypsin (SigmaAldrich), a serine protease that cleaves after tryptophan, tyrosine, phenylalanine and leucine residues.

The native enzyme and the R64W variant were compared, as were the D190A and D190F proteins and their R64W-containing double variants. The native, D190A and D190F proteins showed a fragment at approximately 57 kDa that was absent from the proteins containing the R64W substitution (Fig. 3-11). No other differences between any of the protease profiles of the proteins were observed. The elimination of only 2-4 kDa from the proteins suggests either a single amino-terminal or carboxy-terminal cleavage event or even smaller cleavages at both termini.

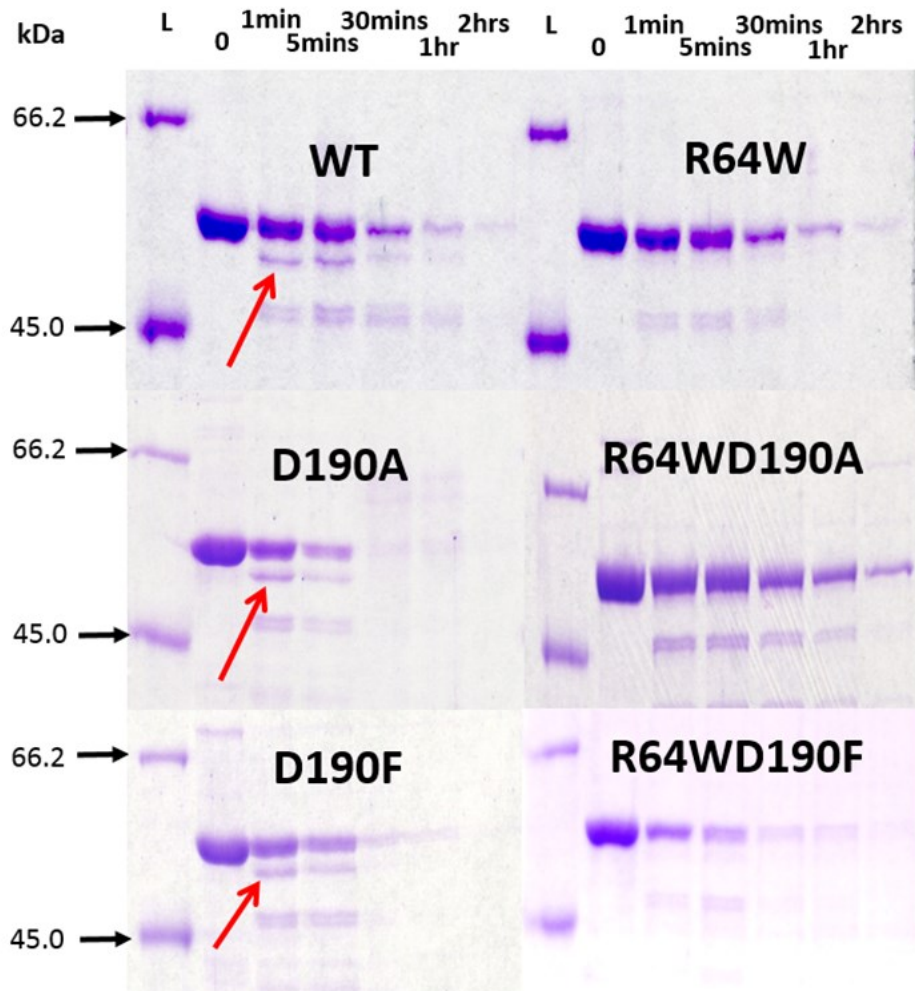


Figure 3-11: Proteolysis of native and variant tRNA nucleotidyltransferases using α -chymotrypsin. Electrophoresis of each proteolytic digest was carried out separately and each gel image was cropped to prepare this figure. The extra fragment seen in the native, D190A and D190F proteins, but not in the R64W, R64WD190A or R64WD190F proteins is marked with an arrow.

3.9.2 Identifying the new chymotryptic cleavage site

Mass spectrometric and computational analyses were carried to determine the difference between the proteins with and without the R64W change. This analyses was carried out by Tian Lai Guan. The bands of interest (intact and truncated native enzyme bands) were excised from the SDS-PAGE gel and an in-gel digestion procedure was carried out using trypsin. The peptides generated from the tryptic digestion of the intact and truncated native enzyme were carried forward for mass spectrometric (Orbitrap) analysis and the results were further analyzed to eliminate the common fragments. Gel images before and after excision of bands of interest have been added to the Appendix (Fig. 7-4).

After thrombin cleavage during the protein purification to remove GST a 'GS' overhang is left on the N-terminus of the target protein (Feeney *et al.*, 2006) and taking that into account, this analysis (Appendix, Fig. 7-5) suggested that both the intact and truncated native enzymes contained similar common fragments. According to the SDS-PAGE results (Fig. 3-11) a clear difference in size between the two fragments is observed but this analyses suggests that it's still uncertain to understand how the extra fragment was generated.

4.0 DISCUSSION

This study is a modest contribution to the field of ongoing research about the yeast tRNA nucleotidyltransferase, a class II nucleotidyltransferase enzyme responsible for the stepwise addition of cytidine-cytidine-adenosine to the 3'-OH end of immature tRNA (Morris and Herbert, 1970). Here, we studied the significance of residues E189 and D190 to better understand the function of motif C; and the significance of residue R64 in motif A to clarify if there was a link between motifs A and C that helps with catalysis. An implication of these findings also further verifies the temperature-sensitive (ts) phenotype exhibited by mutants corresponds to the poor activity of the variants.

4.1 The role of motif C

Based on sequence comparisons we first proposed that residue E189 in the *S. cerevisiae* tRNA nucleotidyltransferase is equivalent to D128, D125 and D139 in the *Aquifex*, *Bacillus* and human tRNA nucleotidyltransferases, respectively (Shan *et al.*, 2008). Using the available crystal structures of these three enzymes (Fig. 4-1) we further suggested that E189 in yeast plays the same role as these residues and stabilizes a flexible β -turn in motif C (Shan *et al.*, 2008).

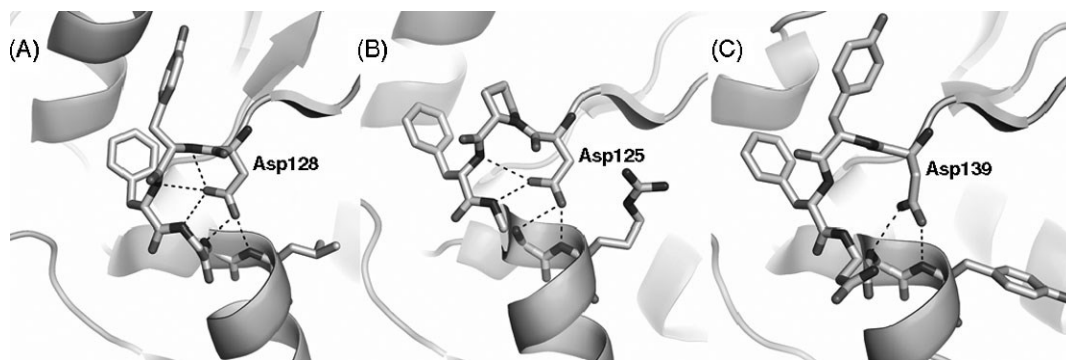


Figure 4-1: The region adjacent to the residue corresponding to *S. cerevisiae* Glu189 in the crystal structures of (A) *A. aeolicus*, (B) *B. stearothermophilus* and (C) human tRNA nucleotidyltransferases (Shan *et al.*, 2008). Each image is centred on the α -carbon of the labelled Asp (equivalent to *S. cerevisiae* Glu189) and the depth is clipped to a 16 Å wide slab. This Asp and the subsequent five residues in each structure are shown in stick representation and shaded according to element to emphasize atomic positions. Dotted lines represent interatomic distances of ≤ 3.51 Å.

The temperature-sensitive phenotype, loss of activity, reduced thermal stability, and reduced tRNA binding in variant enzymes as compared to the native enzyme supported this important role for E189 in the structure and function of the yeast tRNA-NT. We subsequently proposed that replacing E189 with a larger hydrophobic (*e.g.*, phenylalanine) or positively charged residue (*e.g.*, lysine) resulted in a reorganization of the protein around motif C which led to all of the changes that we observed (Shan *et al.*, 2008). We then showed that changing E189 to arginine (another large residue) also generated a temperature-sensitive phenotype consistent with this hypothesis (Goring *et al.*, 2013).

More recently, Ernst *et al.* (2015) have shown the importance of D139 in the human enzyme by showing a 15-fold drop in the rate of AMP addition to a tRNA-CC template when this aspartic acid residue is converted to alanine. This amino acid substitution, however, does not alter the K_m for ATP suggesting that the reduced catalytic activity is linked to changes in the structure of the active site and not simply to substrate (ATP) binding. These data are in good agreement with the role of the aspartate residue at position 139 forming two hydrogen bonds with the backbone $N\alpha$ positions of glycine 143 and tyrosine 144 as shown in Fig. 4-1. These authors argue that removing these hydrogen bonds by converting this aspartate to alanine destabilizes this interaction mediated by motif C and allows for a reorganization of the catalytic head domain of the protein (Fig. 4-2).

Specifically, they used EPR spectroscopy to monitor the arrangement of the protein to suggest that a flexible loop (blue in Fig. 4-2) which forms a salt bridge to glutamate 166 (stick representation, orange) located in motif D is lost when D139 is converted to alanine (stick representation, red), removing the stabilizing hydrogen bonds to glycine 143 and tyrosine 144. The loss of this stabilizing salt bridge between the flexible loop and E166 allows the catalytic head domain to rotate from its initial position such that the active site structure is altered to reduce catalytic efficiency. Based on their EPR analyses Ernst *et al.* (2015) suggest that upon tRNA binding to the catalytic core there is an expansion of about 4 Å of motif C like a 'spring' (Fig. 1-7) leading to accommodation and organization of the remaining substrates (Ernst *et al.*, 2015) and that the rearrangement resulting from the D139A substitution interferes with this process. Therefore, this model based on the human enzyme is fully consistent with our data suggesting

that motif C plays a role in yeast tRNA-NT activity. If these hydrogen bonds between D139 and the main chain at amino acids 143 and 144 in the human enzyme are important to the overall organization of the protein then any changes that remove these hydrogen bonds should be linked to changes in the structure and function of the protein.

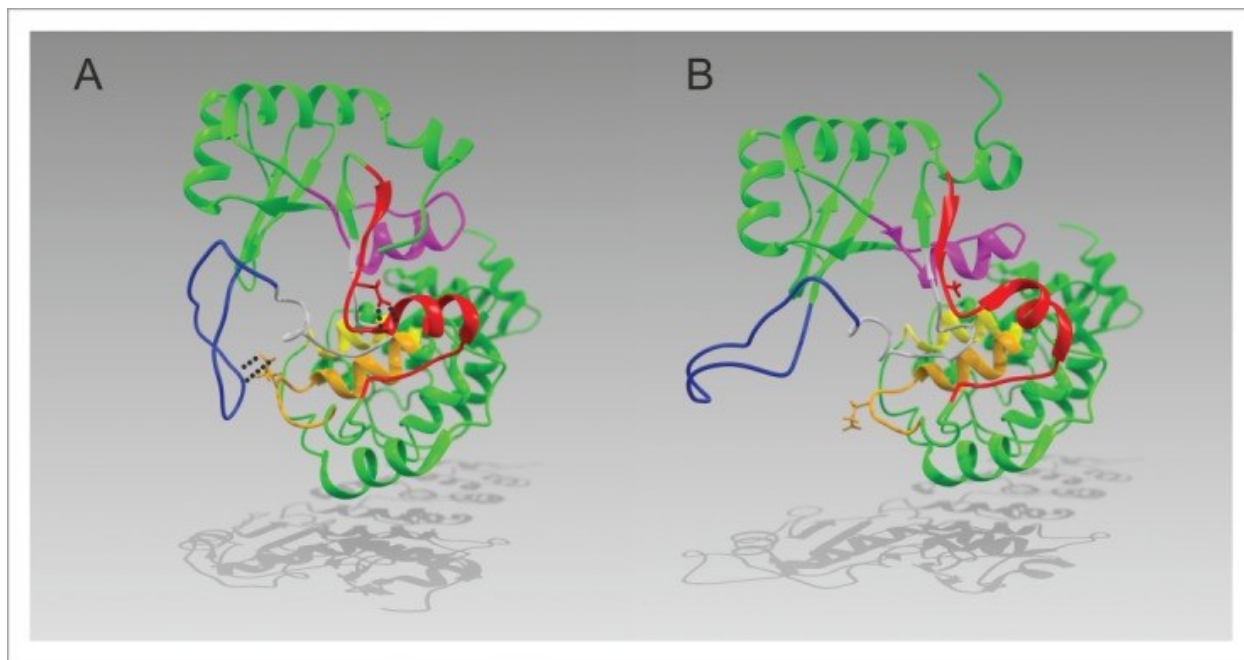


Figure 4-2: Proposed structural model derived from the comparison of the differences between native and D139A variant human tRNA nucleotidyltransferases as revealed after a 7.5 ns MD simulation (YASARA) (Ernst *et al.*, 2015). (A) In the native enzyme the aspartate residue at position 139 (stick model, red) forms two hydrogen bonds with the backbone N α positions of glycine 143 and tyrosine 144, stabilizing the α -helical conformation of motif C and ordering a flexible loop (blue). (B) In the D139A variant, these hydrogen bonds are lost and ultimately the position of the flexible loop and the organization of the active site is changed.

Once again, our studies on the yeast enzyme are entirely consistent with this. Our previous data (Shan *et al.*, 2008) had shown that both enzyme activity and thermal stability were reduced to varying degrees when E189 in the yeast enzyme was converted to phenylalanine, lysine, histidine or glutamine. Similarly, the fluorescence spectra of all of the new variants tested here showed (Table 3-2), showed a red shift (when excited at 280 nm) indicating solvent exposure of one or

more tryptophan residues (Creighton, 1989). It is surprising the same effect did not repeat on the 295 nm spectra.

We selected amino acids to substitute for the glutamate at position 189 to alter the size of the side chain and its hydrogen bonding potential. So while in these cases the hydrogen bonding potential is changed there also is a potential role of steric influences. Here we show that the loss of activity and the temperature-sensitive phenotype associated with the E189F change results from an apparent almost 100-fold drop in catalytic activity with no apparent change in K_m for ATP, CTP or tRNA binding (Tables 3-4 to 3-6). Similarly, there is an approximately 20 to 100-fold drop in catalytic activity in the E189Q variant (Tables 3-4 to 3-6). In both cases it is catalytic activity that is most dramatically affected and we have argued (Shan *et al.*, 2008) that this loss in catalytic activity (but not substrate binding) results from a destabilizing of the β -turn which is supported by motif C such that the active site loses its optimum configuration. Not surprisingly, the more dramatic drop in catalytic activity seen in the E189F variant also is manifested in the more serious temperature-sensitive phenotype seen *in vivo* (Shan *et al.*, 2008).

The differences seen when a phenylalanine or a glutamine is substituted at this position could result either from the altered hydrogen bonding potential of these two amino acids or steric differences based on the differences in size of these amino acids. While phenylalanine is much larger and lacks any potential hydrogen bonds with the main chain amino acids in this turn, glutamine is more similar in size to the glutamate found initially at this position and also can form some hydrogen bonds. To try to tease apart the role of steric concerns and hydrogen-bonding interactions we replaced glutamate 189 with alanine. As with phenylalanine, the hydrogen bonding potential of the side chain will be eliminated but in the case of alanine the size of the side chain (88.6 cubic Angstroms) is much less than that of phenylalanine (189.9 cubic Angstroms). The dramatic reduction in catalytic activity (up to 650 fold) seen in this variant (Tables 3-4 to 3-6) supports the idea that hydrogen bonding is the more important role of this residue.

Interestingly, while most variants exhibited similar biophysical characteristics to the native enzyme (Fig. 3-4 to 3-6), the E189A variant consistently produced different results including an

altered CD spectrum suggesting a loss of α -helical character. Moreover, the E189A variant proved the most difficult to isolate suggesting increased instability during preparation (Fig. 3-1). However, in an apparent contradiction to this, the thermal stability of the E189A variant was found to be the highest (Table 3-1). This apparent contradiction may be explained if it reflects a three-state equilibrium as was observed for the *Arabidopsis* tRNA-NT (Leibovitch *et al.*, 2013) indicating that there is an unfolding intermediate as well as protein aggregation during thermal denaturation.

In summary, our earlier data (Shan *et al.*, 2008) and that presented here through amino acid substitutions at position 189 support the model of Ernst *et al.* (2015) suggesting that motif C is involved in coordinating the arrangement of catalytic residues in the active site and may function like a spring or pivot allowing motion of the head to orient active site residues appropriately to allow the different catalytic events (first CMP addition and subsequently AMP addition) to occur.

Ernst *et al.* (2015) suggest, based on sequence alignments that they generated and from the outcome of their study involving D139, they proposed yeast residue corresponding to the human D139 is actually D190. As there is no yeast crystal structure, we must entertain this possibility. Therefore, we introduced either a phenylalanine or an alanine in place of the aspartate at position 190. D190A or D190F variants showed biophysical characteristics (CD, thermal denaturation or fluorescence studies) similar to those of the E189 variants. However, their corresponding mutants not only exhibited the temperature-sensitive phenotype but the D190F variant was unable to grow in the presence of FOA at the permissive temperature (Fig. 3-1). As we noted a correlation between the temperature-sensitive phenotype and the catalytic activity of the E189 variants, we wanted to see if such a correlation was found with the D190 variants. Similar to the E189 variants there was no dramatic change in K_m value for any substrate (always less than a 4-fold change) but there was a reduction in catalytic activity of at least 100-fold for the D190F variant and on the order of 10-fold for the D190A variant (Tables 3-4 to 3-6). This is intriguing as these reductions in catalytic activities are reversed as compared to the E189F and E189A variants where the more dramatic reduction in activity was seen with the E189A variant. A possible reason for such occurrence could simply be that phenylalanine being a larger molecule is able to affect both the positions 189 and 190; whereas, alanine is significantly smaller in size

and does not. This indicates that E189 corresponds to D139 (unlike proposed by Ernst *et al.*, 2015) and the loss of potential hydrogen bonds as shown in Figure 4-1, could be the reason why D190A is comparatively way more active than the E189A variant.

```

S. cerevisiae      GTPEEDALRR  DATLNALFYN  I----HKGEV  EDFTKRGLQD  LKDGVLRTPL
C. glabrata      GTPEEDALRR  DATLNALFYN  I----QQDAV  EDFTKRGWQD  LQDGVLRTPL
K. lactis        GTPYDDAMRR  DATLNAMFYN  I----TEDKI  EDFTKKGFD  LNDGILRTPL
L. albus         GTPEEDAYRR  DLTINSLFYN  I----NTDSV  EDFTKRGISD  LKSGKIVTPL
A. thaliana     GTAKDDAFRR  DLTINSLFYN  I----NSGAV  EDLTERGIDD  LKSGKIVTPL
B. stearothermophilus -SLEEDLKRR  DFTMNAIAMD  E----YGTII  DPF---GGRE  AIRRRIIRTV
E. coli          VTLEDDLKRR  DFTINALAQD  D----NGEII  DPYNGLG--D  LQNRLLRH-V
A. aeolicus     ASLKEDLIRR  DFTINAMAI  VNLEDYGTLI  DYF--GGLRD  LKDKVIRV-L
H. sapiens      TDWQKDAERR  DLTINSMFLG  F----DGTLF  DYFN--GYED  LKNKKVRF-V
      .*: ** *:*:*: : : : * : : :

```

Figure 4-3: ClustalW alignment of tRNA nucleotidyltransferase sequences optimized manually (Shan *et al.*, 2008). Class II enzymes shown to be active are listed. Only the residues corresponding to amino acids 163–208 of the *S. cerevisiae* sequence flanking the conserved acidic residue (Glu189) in yeast (bold) are shown. (*), amino acid identity; (:), strongly conserved amino acids; (.), weakly conserved amino acids.

Therefore, it is apparent that both E189 and D190 are important in motif C. Similar phenotypes and biophysical and biochemical characteristics are seen when either of these positions is altered. Based on our alignments (Fig. 4-3) perhaps the glutamic acid is needed at position 189 because the predicted loop or turn is larger in this protein than in the human enzyme (Shan *et al.*, 2008). The yeast and plant enzymes that we have studied have at least two additional amino acids between the potential hydrogen bonding residue and the glycine residue whose main chain nitrogen is involved in this hydrogen bond. The sequence alignments also suggest that the residue adjacent to the acidic residue involved in forming the hydrogen bond is variable (aspartate in fungi and plants, proline in *B. stearothermophilus* and *E. coli*, and tyrosine in *A. aeolicus* and humans) but that the next residue is a large hydrophobic residue (typically phenylalanine or tyrosine). It might be interesting to characterize other enzyme variants with changes at this position.

4.2 The role of R64 in enzyme function

As the yeast tRNA-NT is modeled based on the human enzyme (Fig. 4-3) it is apparent that motif C is in a position to interact with motif A. Based on our genetic, biophysical and biochemical data on the yeast enzyme we were the first to propose a relationship between these two motifs (Goring *et al.*, 2013). Specifically, we showed that changing the arginine residue found at the beginning of motif A, to tryptophan suppressed the ts phenotype that resulted when the glutamate residue at position 189 in motif C was converted to lysine or phenylalanine (Goring *et al.*, 2013). R64 is located 17 residues upstream of the two conserved glutamate residues (Fig. 4-4), thus we proposed it plays an important role in catalysis (Fig. 1-4). In subsequent studies, Ernst *et al.* (2015) used a different approach to show that mutations in motif C of the human enzyme cause a reorganization of the active site of the enzyme which possibly could alter the interplay of motifs A and C. Site-directed mutagenesis experiments in motif A from a number of organisms have revealed the essential role of this motif and especially these two glutamate residues in enzyme activity (Steitz, 1998; Li *et al.*, 2002; Xiong *et al.*, 2003) and cell viability (Hanic-Joyce and Joyce, 2002).

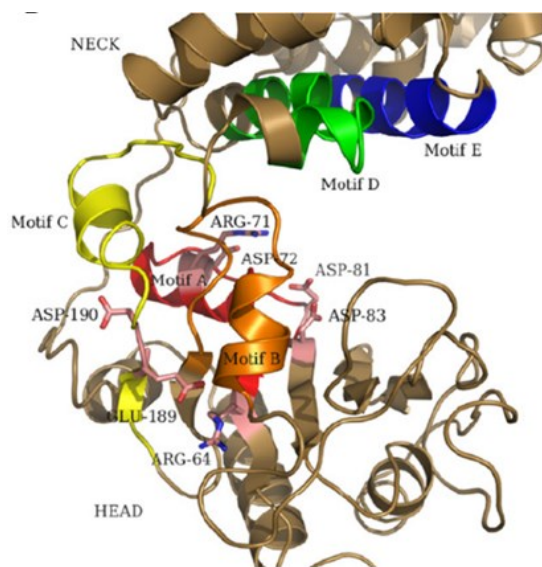


Figure 4-4: Conserved motifs of yeast tRNA-NT showing portions of the head and neck domain (Goring *et al.*, 2013). Each motif has been color coded and labelled, while some important residues are labelled as well.

While the arginine at this position in motif A is conserved in the yeast and human proteins there is a tyrosine at the corresponding position in the bacterial enzymes for which crystal structures have been solved (Fig. 4-5).

```

Aeolicus    --MVGQIAKEMGLRAYYIVGGVVRDILLGKEVWDVDFVVEGN-----AIELAK
Thermotoga --LLGKFGDEVNMPVYVVGGFVRDILLGIKNLDIDIVVEGN-----ALEFAE
Bacillus   --IIQQLKQHG-YDAYFVGGAVRDLLGRPIGDVDIATSAL-----PEDVMA
yeast      LYNQKYHNKPEPLTLRITGGWVRDKLLGQGSHDLDIAINVMSGEQFATGLNEYLQQHYAK
human      LKSLTELFVKENHELRIAGGAVRDLLNGVKPQDIFATTAT-----PTQMK
           . . * * * * * * * * * * * * * * * * * * * * * *

```

Figure 4-5: Alignment of the region around motif A (bold) in five class II tRNA nucleotidyltransferase sequences from different organisms (adapted from Goring *et al.*, 2013). The crystal structures of all of these enzymes except for yeast have been solved. R64 and A85 in the yeast enzyme and the corresponding positions in the other enzymes are shown in red. Note: (*) amino acid identity, (:) strongly conserved amino acid and (.) weakly conserved amino acid.

An examination of the available human crystal structure (Augustin *et al.*, 2003) revealed that this arginine is positioned in the first β -strand of the only β -sheet found in the human tRNA-NT (Fig. 4-6) and that this arginine is involved in two hydrogen bonds with both the backbone amide and carbonyl groups of the alanine residue indicated above as part of this β -sheet. This alanine, near the end of the β -sheet abuts the flexible loop that is found between motifs A and B in the tRNA-NT and is required for switching the specificity of the nucleotide binding pocket from CTP- to ATP-recognition during tRNA extension (Hoffmeier *et al.*, 2010). R64 of the yeast tRNA-NT corresponds to this arginine in the human tRNA-NT (Fig. 4-4). Here, we show that converting this arginine to tryptophan in the yeast enzyme results in no major changes in protein structure (Fig. 3-4, 3-6 and Table 3-2), catalytic activity (Fig. 3-7 and Tables 3-4 to 3-6), thermal stability (Fig. 3-5 and Table 3-1) or cell viability (Fig. 3-1). We also previously used site-directed mutagenesis to change this arginine to glutamate and the cells remained viable (Goring *et al.*, 2013). As seen in Fig. 4-4, the bacterial enzymes for which crystal structures have been solved have a tyrosine at this position. Taken together all of these data suggest that an arginine is not required. Interestingly, the tyrosine in the *B. stearrowthermophilus* tRNA-NT at the corresponding position

forms the same hydrogen bond with the alanine at the end of motif A (Li *et al.*, 2002). So perhaps a basic, acidic or primarily hydrophobic amino acid will work at this position as long as it has a potentially hydrogen bond donating heteroatom placed appropriately at or near alanine at the juncture of the β -sheet and the flexible loop.

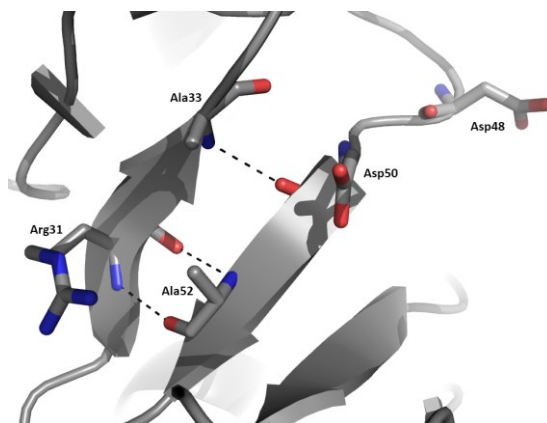


Figure 4-6: Hydrogen bond Interactions of Arg31 and Ala52 (stick conformation) to form part of the only β -sheet found in the human tRNA nucleotidyltransferase. It also includes the DxD region (Asp48 and Asp50) which is located very close to both Arg31 and Ala52, and Asp50 is involved in a potential hydrogen bond with Ala33. The image was generated via PyMOL (Schrodinger) using the crystal structure of the human tRNA-NT (PDB: 1OU5) with a 16 Å wide slab and the dotted lines represent interatomic distances of ≤ 3.51 Å.

If maintenance of this flexible loop is defined in part by this hydrogen bond, and the flexible loop is involved in allowing the conformational change required for the shift of the enzyme from CTP accepting to ATP accepting then changing the amino acid at this position, but maintaining the hydrogen bond should not dramatically change the ability of the enzyme to accept CTP and subsequently ATP. When the tRNA-N template was used (Fig. 3-7) it is apparent that the R64W variant shows slightly less activity than the native (R64) enzyme with approximately twice as much unreacted template and only 20% complete product with the lowest enzyme amount (1 ng) tested (Table 3-3). With an intermediate enzyme amount (5 ng) it is apparent that while the native enzyme has converted 80% of substrate to complete tRNA-NCCA product (Fig. 3-7), the R64W variant has converted only about one third of the substrate to tRNA-NCCA product with some tRNA-NCC and tRNA-NC intermediates accumulating (Table 3-3). Finally with the highest

amount of protein both enzymes show more than 80% of substrate converted to fully extended tRNA-NCCA product with no apparent intermediates (Fig. 3-7). From these data one may suggest that the R64W variant is slightly less efficient than the native enzyme, but it is difficult to say if the reduced activity reflects tRNA binding, CMP incorporation or AMP incorporation.

Given the complexity of this assay, where CTP, ATP and tRNA are substrates, it is difficult to define specific kinetic parameters for this assay. Therefore, kinetic parameters were defined in simplified reactions containing a specific tRNA template (either tRNA-NC or tRNA-NCC) for the incorporation of a single CMP (in the first case) or AMP residue (in the second case). Based on this characterization, tRNA binding was not affected as the K_m s for tRNA binding (within experimental error) and the turnover numbers for the native and R64W enzymes were the same (Table 3-4). When the tRNA-NC template was used and CMP incorporation measured, the K_m for CTP binding suggested an approximately three fold tighter binding of CTP in the R64W variant as compared to the native enzyme although the turnover number showed only a slight decrease in the variant (Table 3-5). Perhaps the potential slightly tighter binding of CTP is reflected in the presence of tRNA-NC and tRNA-NCC intermediates in the R64W reaction at 5 ng of protein that are absent from the native enzyme (Fig. 3-7). Finally, when the tRNA-NCC template was used to measure AMP incorporation, both the K_m s and turnover numbers are essentially the same. Based on these data, it appears that converting the arginine at position 64 to tryptophan has no effect on tRNA or ATP binding, but may have some effect on CTP binding.

To address further the binding of ATP or CTP to the enzyme we carried out fluorescence quenching experiments using increasing amounts of ATP or CTP. From these data (Table 3-8), we saw an approximately three-fold change in K_d for CTP consistent with what we saw in the kinetic analysis. In contrast, the K_d for ATP also changed about three fold although the K_m values for ATP with both proteins were the same (Table 3-6). Given how the fluorescence quenching was carried out (*i.e.*, in the absence of tRNA) it is difficult to make any firm statements based on these results. It would be better to do these experiments in the presence of the various tRNA substrates, but these substrates are on the order of 25 000 Da and serve to quench the fluorescence of the protein (Shan *et al.*, 2008) making this type of experiment difficult.

As R64 is linked to motif A which contains the two conserved aspartate residues, involved in coordinating the catalytic magnesium ions (Fig. 1-4) we wished to see if the R64W variant affected how these residues functioned. We reasoned that it was possible for the conversion of an arginine to tryptophan to have altered the organization of the β -sheet of which it is a part so that the orientation of the two aspartate residues changes the orientation of the metal ions and alters enzyme activity. We previously had shown that the R64W variant like the native enzyme can misincorporate AMP at the first position or CMP at the third position of the CCA sequence *in vitro* (Goring *et al.*, 2013). This raised the possibility that if the two aspartates were reoriented in space, then the metal ions were moved in space such that this allowed for an incorrect nucleotide triphosphate to fit into the space that resulted. To address this we measured the incorporation of AMP (tRNA-N template) or CMP (tRNA-NCC template) or AMP and CMP (tRNA-N template) in the presence of different metal ions. We reasoned that if the spacing of the aspartate residues was changed, then using larger metal ions may compensate for this altered arrangement. We performed these experiments with five ng of the appropriate enzyme but allowed the reactions to go for 20 minutes to increase the amount of product that could be seen.

Similar to what we saw previously with the native enzyme (Goring *et al.*, 2013), ATP was incorporated rather efficiently into the position normally held by the first added CMP and to a much lesser degree into the position normally occupied by the second CMP (Fig. 3-8). In contrast, we observed an even more efficient incorporation of a second AMP to generate a tRNA-NAA product with the R64W variant. When we looked at CMP incorporation into the tRNA-NCC template we saw that both the native and R64W variant could incorporate CMP into the third position and in fact even further generating tRNA-NCCCC products. Extension of the template beyond the usual termination point was even more apparent when the tRNA-N template was used with both ATP and CTP and in this case the addition of extra bases was seen best with the R64W variant. Other studies which reported extension beyond the third position mentioned that those tRNAs are dysfunctional and unstable (Yamashita and Tomita, 2016) and usually a second repeat of CCA is only added to initiate their degradation (Kuhn *et al.*, 2015).

When cobalt was used in the place of magnesium with the native enzyme we saw less efficient use of the tRNA-N template, but any of the template that had a first AMP incorporated served as

a better substrate for the incorporation of a second AMP residue than was seen when magnesium was used (Fig. 3-8, Table 3-7). This increase in the efficiency of misincorporation was also seen with the R64W variant. There were no major differences in CMP, or AMP and CMP incorporation in the other cobalt samples for the native or R64W variant as compared to the reactions containing magnesium. This raises the question of why the presence of the slightly larger metal ion affects the incorporation of AMP more at the first and second positions than of AMP or CMP at subsequent positions.

When either manganese or calcium were used in place of magnesium as the metal ion the reactions showed lower levels of misincorporation for both the native and R64W variant (Fig. 3-8, Table 3-7). This likely reflects the reduced efficiency with which the enzymes can use these larger ions more than an increase in specificity. That increasing the size of the ions to that of manganese or calcium effects both the native enzyme and the R64W variant in the same way suggests that the organization of this region of the active site has not been altered to any major degree in the R64W variant as compared to the native enzyme. Again this supports the general idea that as long as the hydrogen-bonding potential of the residue at position 64 is maintained the organization of the active site is generally conserved.

As Klemperer and Haynes (1967) have shown previously that using manganese ions instead of magnesium ions, resulted in increased misincorporation of UMP and AMP in place of CMP we decided to compare the misincorporation of UMP and GMP by the native and R64W variants. Rather than compare magnesium and manganese we selected calcium, as it was the largest ion among those we tested. In the presence of magnesium and with the tRNA-N template and the native enzyme we saw AMP and CMP incorporation as seen previously, a very small amount of GMP incorporation at the first position and UMP incorporation efficiently at the first position and to a lesser degree at the second position. With the tRNA-NC template, we saw two AMPs incorporated, likely three CMPs, a small amount of one GMP and slightly more UTP. Finally, with the tRNA-NCC template we saw AMP incorporation as expected, some CMP incorporation, little GMP addition and UMP incorporation as efficient as for CMP at this position. These data are generally as expected with the purine residue most efficiently fitting in place of the required

purine and the pyrimidine replacing the normal pyrimidine, however, the more efficient addition of UMP than GMP to the tRNA-NCC template is unexpected.

The results with the R64W variant again almost parallel exactly the results with the native enzyme. These data again support the idea that as long as the hydrogen bonding potential of the residue at position 64 is maintained the activity of the enzyme remains similar. As seen previously, both enzymes work very poorly with calcium ions and so this dramatically reduced activity does not allow misincorporation to be detected.

While neither the CD nor fluorescence spectroscopy showed any major changes in protein structure for almost all of the variants, we thought that we would try a different approach to see if we can see any changes in the R64W variant versus the native enzyme. Therefore, we digested the protein with α -chymotrypsin hypothesizing that if there were any structural changes they may either reveal or sequester a cleavage site. The native enzyme showed an extra fragment (56-58 kDa) on SDS-PAGE that was absent from the R64W variant (Fig. 3-11). A possible explanation for this is that a conformational change resulted in the burial of a cleavage site, which may suggest a change in the orientation of the protein caused by the R64W substitution. Given that the protein contains 110 residues that could serve as sites of cleavage and they are scattered over the entire protein the absence of the 56-58 kDa band suggests that a site is near one or the other end of the protein (approximately 60 kDa). Unfortunately, when the 56-58 kDa fragment was isolated and subjected to mass determination by mass spectrometric analysis it was not clear of where the difference was with the as the original fragment. It is important to remember that the conversion of arginine to tryptophan at position 64 could introduce a new chymotrypsin cleavage site. This extra site may lead to a more rapid degradation of the protein, which also could explain the loss of the apparent 56-58 kDa fragment.

In summary, it can be deduced from all of the observations of these and previous studies that the native and R64W enzymes share very common features making it difficult to separate them. However, slight difference in overall efficiency and in terms of misincorporation studies, the reorganization of the head domain is evident which may be the primary reason of how the R64W double variants exhibits restoration of activity.

A temperature-sensitive yeast strain which was unable to grow at 37°C (restrictive temperature) was first isolated by Aebi *et al.* (1990). In a subsequent study involving substitution mutations at glutamate 189 we showed such phenomenon that occurred when the enzymatic activity was as low as 4% compared to the native enzyme (Shan *et al.*, 2008). Interestingly, such low enzymatic activity is still enough to keep the mutant cells alive at 22°C (permissive temperature). Later, we discovered through UV mutagenesis studies and sequencing that the temperature-sensitive mutants can grow at 37°C when an intragenic suppressor in the form of R64W substitution was present (Goring *et al.*, 2013). Here we demonstrate that both the D190A and D190F variants are unable to grow at the restrictive temperature, in fact the D190F variants lacks growth at the permissive temperature as well (22°C). Unsurprisingly, the R64W double mutants of both positions 189 and 190 were not only able to survive in the permissive and restrictive temperatures, but the enzymatic activity of their corresponding variants also showed improvement.

It was primarily deduced that the exhibition of the temperature-sensitive phenotype was due to the mutant cells inability to cope up with the demand for mature tRNA, thus affecting protein synthesis negatively (Peltz *et al.*, 1992). This analogy is in good agreement with studies demonstrating defense mechanisms of how organisms adapts to sudden rise in temperature; and one such study involving yeast as the model organism shows that the expression of proteins such as heat shock proteins (Hsp) are upregulated upon detection such stressful conditions by aiding growth and cell survival (Verghese *et al.*, 2012). This ensures why the wildtype yeast cells are viable at the restrictive temperature (Fig. 3-1). Previously, we associated the temperature-sensitive phenotype to lower thermal stability of enzymes, thus indicating a lower remaining α -helical character at the melting temperature (Goring *et al.*, 2013); however, this study demonstrates no such trend since the variants E189A and E189Q were found to be more thermally stable than the native enzyme (Fig. 3-5 and Table 3-1).

We barely deciphered any difference in terms of enzyme function between the native and R64W enzymes, yet the latter is able to restore enzymatic activity in the poorly active E189 and D190 variants. From the scope of this study and also as evident in Goring *et al.* (2013), it seems that the restoration of activity is caused due to the reorganization of the head domain by substituting

arginine 64 to tryptophan is the only difference seen that suppresses the temperature-sensitive phenotype. It is difficult to explain why D190F mutant cells exhibited low or no growth at the permissive temperature especially compared to the other poorly active E189F or E189A variants, which exhibits even lower activity but still survives in the same condition (Fig. 3-1, 3-7 and Table 3-3). The D190F variant did not show any difference in its biophysical characteristics (Fig. 3-4 to 3-6) and it is very likely that other factors may be involved alongside poor activity that leads to no growth at the permissive temperature. Perhaps, this substitution creates an opportunity for protein-protein interactions of the tRNA-NT with other protein that leads to cell death and is yet to be explored. Since that unknown protein is not present *in vitro*, it could be the reason why we are still able to trace amounts of activity.

5.0 CONCLUSION AND FUTURE WORKS

We conducted this study to better understand the role of motif C by specifically defining the roles of residues both glutamate 189 and aspartate 190 using the yeast tRNA-NT as the model enzyme. Substitutions in both positions expressed a temperature-sensitive (ts) phenotype alongside poor enzymatic activity. Introducing a R64W substitution (in motif A), restored enzymatic activity in the poorly active E189 and D190 variants while suppressing their corresponding ts phenotype helping with the demonstrating of any direct or indirect connection between motifs A and C.

From the research that had been conducted, we observed no major structural or stability differences in the variants with substitutions in motif C and the key and crucial difference was observed in the kinetic studies where we demonstrated the effect of altering motif C was mainly on catalysis. The importance of position 189 has already been shown in Goring *et al.* (2013), and a simple substitution from glutamate to glutamine (E189Q) reduced activity between 20-80 fold. However, the outcomes of E189A, and the D190A variant is lack of expressing any similar features it was more likely that E189 in the yeast tRNA-NT corresponds to D139 in the human tRNA-NT. Moreover, the alignment of the sequences of different class II tRNA-NT indicates higher sequence similarity when the aspartates (missing glutamate) are aligned to the glutamates.

Summing up the results, it is clear that both the positions 189 and 190 plays important roles in making motif C help accommodate, organize and orient the substrates correctly near motif A so catalysis is efficient. When either of these important residues are substituted, the overall effect on catalysis is drastic. We also demonstrated that the R64W substitution is able to restore enzyme activity in the D190 variants as well while suppressing their corresponding ts phenotype. We deduced that regardless of being close to the conserved GGxVRD and DxD sequences in motif A, R64 does not have any particular function other than being involved in formation of the signature β -sheet in the head domain, even though our experiments indicate some influences on nucleotide selectivity in the R64W variant. It was primarily hypothesized that R64 and E189 interacts via a salt bridge, and it's disruption was not the reason behind the development of the ts phenotype (Goring, 2011); and from the current study we reensure that the R64W enzyme is very similar to the native enzyme in most aspects that nullifies the salt bridge hypothesis as well.

We proposed that the R64W substitution reorients the head domain just enough so that the restoration of activity is observed for both sets of E189 and D190 variants. However, the R64W substitution by itself (R64W variant) is not a vital factor when motif C is functional, even though a miniscule reduction in catalytic efficiency is evident.

Further investigating the native and R64W enzymes through biochemical analysis using different metal ions as cofactor, we thought the binding pocket might be slightly smaller in the R64W enzyme, which may be due to the reorientation this change causes. From the scope of this study, we reconfirm that the ts phenotype in most cases is linked to the reduction in activity; whereas, the restoration of activity always correlates to the suppression of the ts phenotype.

While this study aims to provide a comprehensive account of the link between motifs A and C to better define the function of the latter, more research is required. To demonstrate why the D190F mutants lacked growth at the permissive temperature, perhaps a throughput mass spectrometric analyses can be carried out. This could help us identify the difference in expression patterns of proteins in the D190F mutant, and compare to other ts mutants. Discovering if by introducing a lysine, tyrosine or even phenylalanine (basic or aromatic residues) at position 64 persists the same effect could be interesting as well. This would further verify the indirect role of this position that comes into play only when motif C is defective and indicating how motifs A and C are indirectly involved.

We investigated the denaturation pattern through monitoring changes in α -helical content since the yeast tRNA-NT like is highly abundant with α -helices. Perhaps, small changes in β -structures due to their rarity in these proteins could not be monitored efficiently with techniques such as FT-IR. This would help identify such structural changes for both the R64W substitution (R64 falls in a β -strand) and in E189 and D190 variants (both located close to a β -sheet). The proteolytic study can be reinvestigated with some other proteases that does not cleave after positive or aromatic residues to see digestion patterns, with a follow up mass spectrometric analysis to explain further the effect of substitutions at positions 64, 189 or 190 in the yeast tRNA-NT.

Lastly, if the crystal structure can be solved for the yeast tRNA-NT through techniques such as X-ray crystallography, more computational approaches would be approachable to get more

qualitative models of the variant enzymes to predict or demonstrate the changes in orientation that led to the reduction and the restoration in activity.

6.0 REFERENCES

- Aebi, M., Kirchner, G., Chen, J. Y., Vijayraghavan, U., Jacobson, A., Martin, N. C., & Abelson, J. (1990). Isolation of a Temperature-Sensitive Mutant With an Altered Transfer-Rna Nucleotidyltransferase and Cloning of the Gene Encoding Transfer-RNA Nucleotidyltransferase in the Yeast (*Saccharomyces cerevisiae*). *Journal of Biological Chemistry*, **265**(27), 16216–16220.
- Arthur, J. (2009). *The role of arginine 244 in Candida glabrata tRNA nucleotidyltransferase*. Concordia University.
- Augustin, M. A., Reichert, A. S., Betat, H., Huber, R., Mörl, M., & Steegborn, C. (2003). Crystal structure of the human CCA-adding enzyme: Insights into template-independent polymerization. *Journal of Molecular Biology*, **328**(5), 985–994.
- Berg, J. M., Tymoczko, J. L., Stryer, L. (2010). *Biochemistry*. W. H. Freeman and Company, New York.
- Betat, H., Rammelt, C., Martin, G., & Mörl, M. (2004). Exchange of regions between bacterial poly(A) polymerase and the CCA-adding enzyme generates altered specificities. *Molecular Cell*, **15**(3), 389–398.
- Betat, H., Rammelt, C., & Mörl, M. (2010). tRNA nucleotidyltransferases: Ancient catalysts with an unusual mechanism of polymerization. *Cellular and Molecular Life Sciences*, **67**, 1447–1463.
- Bradford, M. M. (1976). A rapid and sensitive method for the quantitation of microgram quantities of protein utilizing the principle of protein-dye binding. *Analytical Biochemistry*, **72**(1–2), 248–254.
- Chakraborty, P. K., Schmitz-Abe, K., Kennedy, E. K., Mamady, H., Naas, T., Durie, D., ... Fleming, M. D. (2014). Mutations in TRNT1 cause congenital sideroblastic anemia with immunodeficiency, fevers, and developmental delay (SIFD). *Blood*, **124**(18), 2867–2871.
- Cho, H. D., Verlinde, C. L. M. J., & Weiner, A. M. (2007). Reengineering CCA-adding enzymes to function as (U,G)- or dCdCdA-adding enzymes or poly(C,A) and poly(U,G) polymerases. *Proceedings of the National Academy of Sciences of the United States of America*, **104**(1), 54–59.
- Colasurdo, G. (2011). *The role of arginine 204 in Candida glabrata tRNA nucleotidyltransferase*. Concordia University.
- Creighton, T. E. (1989). *Protein structure: a practical approach*. IRL. Oxford University Press.
- Ernst, F. G. M., Rickert, C., Bluschke, A., Betat, H., Steinhoff, Heinz-Jürgen, & Mörl, M. (2015). Domain movements during CCA-addition : A new function for motif C in the catalytic core of the human tRNA nucleotidyltransferases. *RNA Biology*, **12**(4), 435–446.
- Feeney, B., Soderblom, E. J., Goshe, M. B., & Clark, A. C. (2006). Novel protein purification system utilizing an N-terminal fusion protein and a caspase-3 cleavable linker, **47**(1), 311–318.
- Gasteiger, E., Hoogland, C., Gattiker, A., Duvaud, S., Wilkins, M. R., Appel, R. D., & Bairoch, A. (2005). Protein Identification and Analysis Tools on the ExPASy Server. *The Proteomics Protocols Handbook*, 571–607.
- Goring, M. E. (2011). *Characterization of temperature-sensitivity and its intragenic suppression in Saccharomyces cerevisiae tRNA nucleotidyltransferase mutants*. Concordia University.

- Goring, M. E., Leibovitch, M., Gea-Mallorqui, E., Karls, S., Richard, F., Hanic-Joyce, P. J., & Joyce, P. B. M. (2013). The ability of an arginine to tryptophan substitution in *Saccharomyces cerevisiae* tRNA nucleotidyltransferase to alleviate a temperature-sensitive phenotype suggests a role for motif C in active site organization. *Biochimica et Biophysica Acta - Proteins and Proteomics*, **1834**, 2097–2106.
- Hanic-Joyce, P. J., & Joyce, P. B. M. (2002). Characterization of a gene encoding tRNA nucleotidyltransferase from *Candida glabrata*. *Yeast*, **19**(16), 1399–1411.
- Harper, S., Speicher, D. W., & Ph, D. (2011). *Protein Chromatography*, **681**, 1–15.
- Hoffmeier, A., Betat, H., Bluschke, A., Günther, R., Junghanns, S., Hofmann, H. J., & Mörl, M. (2010). Unusual evolution of a catalytic core element in CCA-adding enzymes. *Nucleic Acids Research*, **38**(13), 4436–4447.
- Kelly, L. A., Mezulis, S., Yates, C., Wass, M., & Sternberg, M. (2015). The Phyre2 web portal for protein modelling, prediction, and analysis. *Nature Protocols*, **10**(6), 845–858.
- Klemperer, H. G.; Haynes, G. R. (1967). Altered Specificity of Transfer-Ribonucleic Acid Nucleotidyltransferase in the Presence of Manganese. *Biochemistry*, **104**, 537-544.
- Kuhn, C., Wilusz, J. E., Beal, P. a, Joshua-tor, L., Kuhn, C., Wilusz, J. E., ... Joshua-tor, L. (2015). On-Enzyme Refolding Permits Small RNA and tRNA Article On-Enzyme Refolding Permits Small RNA and tRNA Surveillance by the CCA-Adding Enzyme. *Cell*, **160**(4), 1–15.
- Leatherbarrow, R. J. (2009). *GraFit Version 7*. Erithacus Software Ltd., Horley, U.K.
- Leibovitch, M., Bublak, D., Hanic-joyce, P. J., Tillmann, B., Flinner, N., Amsel, D., ... Schleiff, E. (2013). The folding capacity of the mature domain of the dual-targeted plant tRNA nucleotidyltransferase influences organelle selection, **412**, 401–412.
- Li, F., Xiong, Y., Wang, J., Cho, H. D., Tomita, K., Weiner, A. M., & Steitz, T. A. (2002). Crystal structures of the *Bacillus stearothermophilus* CCA-adding enzyme and its complexes with ATP or CTP. *Cell*, **111**, 815–824.
- Liu, H., & Naismith, J. H. (2008). An efficient one-step site-directed deletion, insertion, single and multiple-site plasmid mutagenesis protocol. *BMC Biotechnology*, **8**(1), 91.
- Morris, R. W., & Herbert, E. (1970). Purification and characterization of yeast nucleotidyl transferase and investigation of enzyme-transfer ribonucleic acid complex formation. *Biochemistry*, **9**(24), 4819–27.
- Peattie, D. A. (1979). Direct chemical method for sequencing RNA. *Proceedings of the National Academy of Sciences of the United States of America*, **76**(4), 1760–4.
- Peltz, S. W., Donahue, J. L., & Jacobson, a. (1992). A mutation in the tRNA nucleotidyltransferase gene promotes stabilization of mRNAs in *Saccharomyces cerevisiae*. *Molecular and Cellular Biology*, **12**(12), 5778–5784.
- Sambrook, J., Maniatis, T., Fritch, E. F. (1989). *Molecular Cloning* (2nd ed.). Cold Spring Harbor Laboratory Press.
- Sarman, F., Thiffault, I., Weraarpachai, W., Salomon, S., Maftai, C., Gauthier, J., ... Shoubridge, E. A. (2015). The 3' addition of CCA to mitochondrial tRNA^{Ser(AGY)} is specifically impaired in patients with mutations in the tRNA nucleotidyl transferase TRNT1. *Human Molecular Genetics*, **24**(10), 2841–2847.

- Schrödinger. (n.d.). The PyMOL Molecular Graphics System, Version 1.8 Schrödinger, LLC.
- Shan, X., Russell, T. A., Paul, S. M., Kushner, D. B., & Joyce, P. B. M. (2008). Characterization of a temperature-sensitive mutation that impairs the function of yeast tRNA nucleotidyltransferase. *Yeast*, **25**, 219–233.
- Steitz, T. A. (1998). A mechanism for all polymerases. *Nature*, **391**, 231–232.
- Toh, Y., Takeshita, D., Numata, T., Fukai, S., Nureki, O., & Tomita, K. (2009). Mechanism for the definition of elongation and termination by the class II CCA-adding enzyme. *The EMBO Journal*, **28**, 3353–3365.
- Tomita, K., Fukai, S., Ishitani, R., Ueda, T., Takeuchi, N., Vassilyev, D. G., & Nureki, O. (2004). Structural basis for template-independent RNA polymerization. *Nature*, **430**, 700–704.
- Tomita, K., Ishitani, R., Fukai, S., & Nureki, O. (2006). Complete crystallographic analysis of the dynamics of CCA sequence addition. *Nature*, **443**, 956–960.
- Verghese, J., Abrams, J., Wang, Y., & Morano, K. A. (2012). Biology of the Heat Shock Response and Protein Chaperones: Budding Yeast (*Saccharomyces cerevisiae*) as a Model System. *Microbiology and Molecular Biology Reviews*, **76**(2), 115–158.
- Walker, J. M. (2002). *Protein handbook* (2nd ed.), Humana Press.
- Wong, C., Sridhara, S., Bardwell, J. C., Jakob, U. (2000). Heating greatly speeds Coomassie blue staining and destaining. *Biotechniques*, **28**(3), 426–8, 430, 432.
- Xiong, Y., Li, F., Wang, J., Weiner, A. M., & Steitz, T. A. (2003). Crystal structures of an archaeal class I CCA-adding enzyme and its nucleotide complexes. *Molecular Cell*, **12**, 1165–1172.
- Yakunin, A. F., Proudfoot, M., Kuznetsova, E., Savchenko, A., Brown, G., Arrowsmith, C. H., & Edwards, A. M. (2004). The HD domain of the *Escherichia coli* tRNA nucleotidyltransferase has 2',3'-cyclic phosphodiesterase, 2'-nucleotidase, and phosphatase activities. *Journal of Biological Chemistry*, **279**(35), 36819–36827.
- Yamashita, S., & Tomita, K. (2016). Mechanism of 3'-Matured tRNA Discrimination from 3'-Immature tRNA by Class-II CCA-Adding Enzyme. *Structure*, **24**(6), 918–925.
- Yue, D., Maizels, N., & Weiner, A. M. (1996). CCA-adding enzymes and poly(A) polymerases are all members of the same nucleotidyltransferase superfamily: Characterization of the CCA-adding enzyme from the archaeal hyperthermophile *Sulfolobus shibatae*. *RNA*, **2**, 895–908.

7.0 APPENDIX

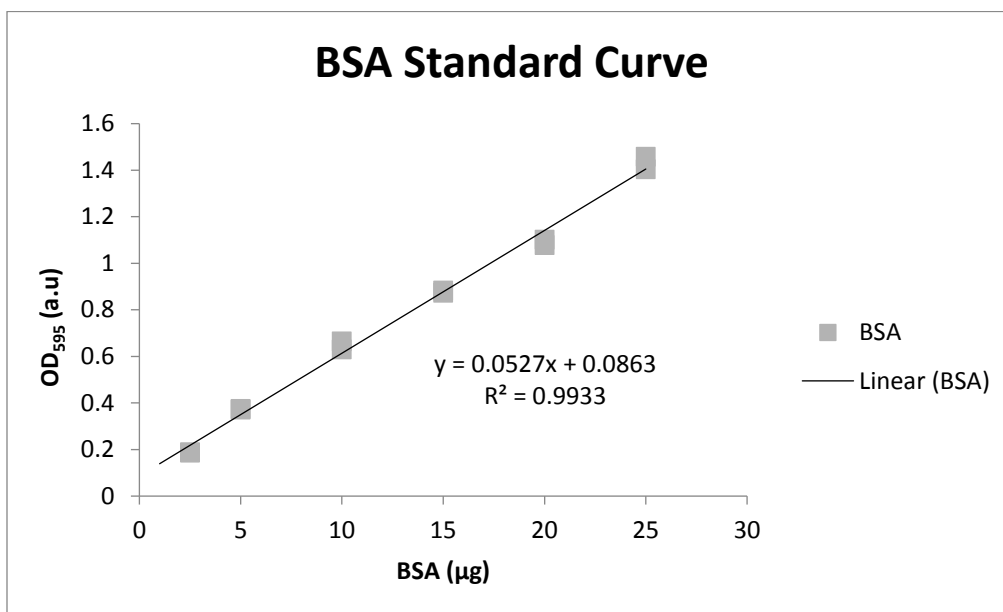


Figure 7-1: BSA standard curve to determine the concentrations of the native and variant tRNA nucleotidyltransferases

Enzyme	Absorbance (a.u.)	Concentration (ng/µL)
Native	0.633	296.39
R64W	0.412	176.57
E189F	0.348	141.88
D190F	0.452	198.26
D190A	0.511	230.25
E189A	0.223	74.11
E189Q	0.287	108.81
R64WE189F	0.238	82.24
R64WD190F	0.442	192.84
R64WD190A	0.466	205.85
R64WE189A	0.572	263.32
R64E	0.3811	159.82

Table 7-1: List of concentrations of native and variant tRNA nucleotidyltransferases determined from Bradford assay

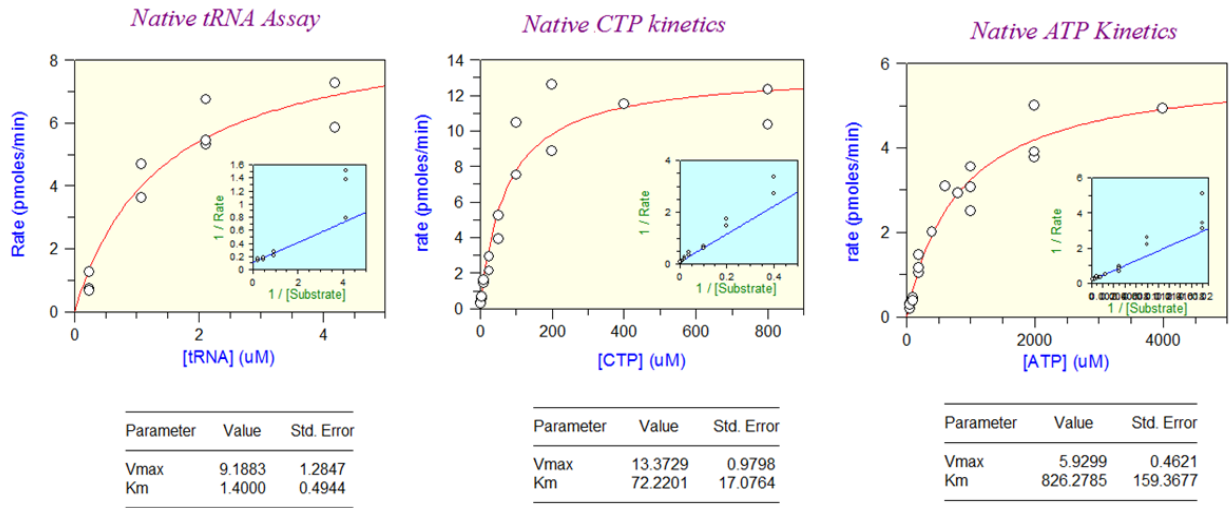


Figure 7-2: Michaelis-Menten graphs of the native enzyme using tRNA, CTP or ATP as variable substrate to determine kinetic parameters.

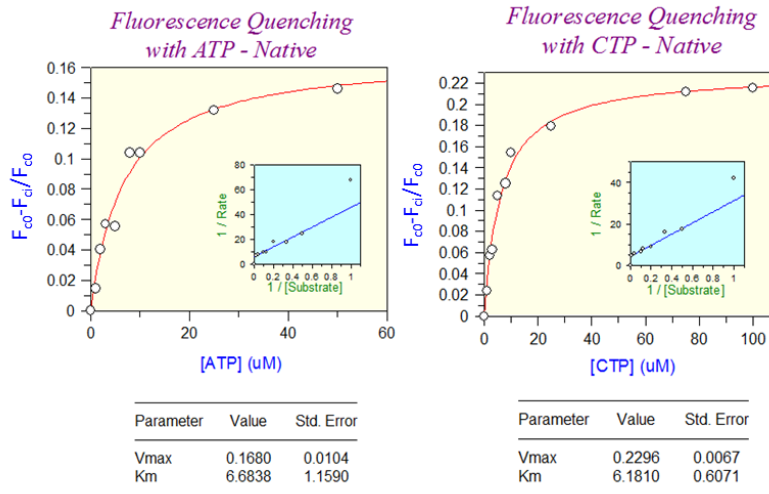


Figure 7-3: Determination of dissociation constant of native tRNA nucleotidyltransferase using fluorescence quenching with ATP or CTP. Note: The K_d is calculated from this relationship and not K_m and the value for V_{max} was used as F_{max} (See Section 2.4.3).

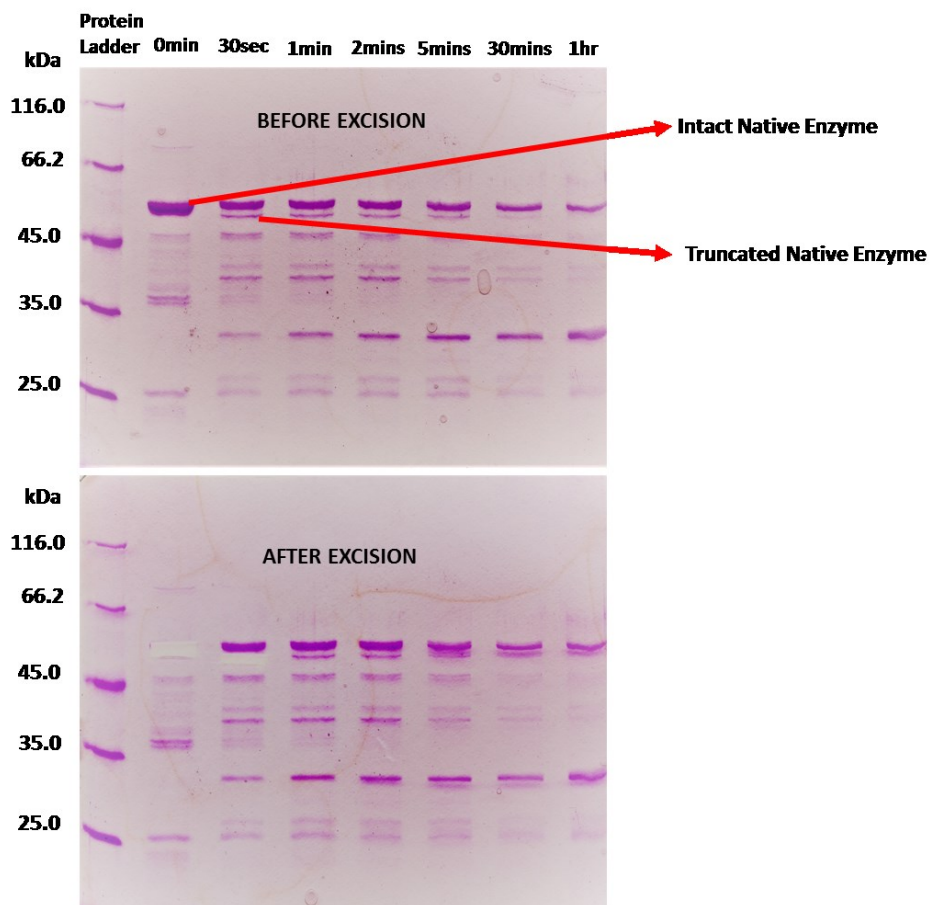


Figure 7-4: Gel images showing excision of bands of interest before trypsin digestion and mass spectrometric (Orbitrap) analysis. The top image is before the excision of the intact and truncated protein bands and the gel image below is after the excision was performed.

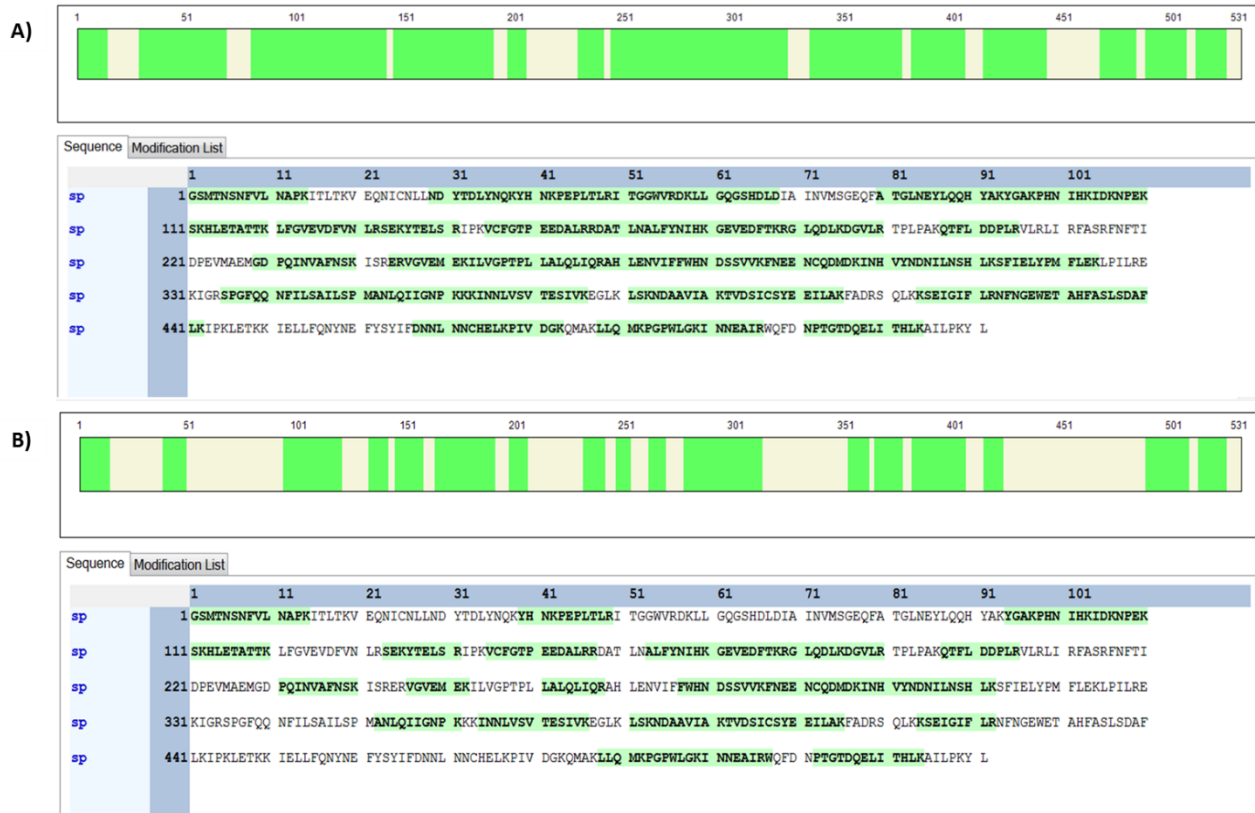


Figure 7-5: Mass spectrometric results generated from SEQUEST search carried out against a *S. cerevisiae* proteome database from UniProt. The green highlighted areas are the common peptide fragments identified from the intact native enzyme (top) and the truncated native enzyme (bottom).

MTNSNFV**L**NAPKIT**L**TKVEQNICN**L**ND**Y**TD**L**Y**N**QKYHNKPEPLTLRITGGWVRDKLLGQ
 GSHDLDAINVMISGEQFATGLNEYLQQHYAKYGAKPHNIHKIDKNPEKSKHLETATTKLF
 GVEVDFVNLRSEKYTELSRI PKVCFGTPEEDALRRDATLNALFYNIHKGEVEDFTKRGLQ
 DLKDGVLRTPLPAKQTFLLDDPLRVLRIRFASRFNFTIDPEVMAEMGDPQINVAFNSKIS
 RERVGVEMEKILVGPTPLALQLIQRAHLENIFFWHNDSVVKFNEENCQDMDKINHVI
 NDNILNSHLKSFIELYPMFLEKLPILREKIGRSPGFQQNFILSAILSPMANLQIIGNPKK
 KINNLVSVTESIVKEGLKLSKNDAAVIAKTVDSICSYEEILAKFADRSQKKSEIGIFLR
 NFNGEWETAHFASLSDAFLKIPKLETKKIELLFQNYNEFYSYIFDNNLNCHLKPVDG
 KQMAKLLQMKPGPWLGGKINNEAIRWQFDNPTGTDQELITHLKAILPKYL

Figure 7-6: Possible cleavage sites of α -chymotrypsin in native tRNA-NT. The portion of the sequence highlighted in yellow indicates majority of the extra fragment generated for the native enzyme (also D190A and D190F). The red highlight indicates possible cleavage sites responsible for extra fragment.



Figure 7-7: Models of native and R64W tRNA-NTs to investigate the possible chymotryptic cleavage site using PyMOL. The left image shows the native enzyme where it shows that R64 is pointing away from the protein core (prefers polar environment). The image on the right depicts R64W protein.